U. S. Department of Commerce
National Oceanic and Atmospheric Administration
National Weather Service
National Centers for Environmental Prediction
5200 Auth Road Room 207
Camp Springs, MD 20746

Technical Note

The Operational North Atlantic Hurricane Wind-Wave Forecasting System at NOAA/NCEP[†].

Jose-Henrique G.M. Alves[°,‡], Yung Y. Chao and Hendrik L. Tolman[°]
Marine Modeling and Analysis Branch
Environmental Modeling Center
Marine Modeling and Analysis Branch

February 2005

[†] MMAB Contribution No. 244.

[°] SAIC/GSO [‡] e-mail: Henrique.Alves@NOAA.gov

This page is intentionally left blank.

Abstract

The North Atlantic Hurricane (NAH) wave model has been developed at the National Centers for Environmental Prediction (NCEP) to produce forecasts of hurricane-generated waves during the Atlantic hurricane season. A detailed description of this model and a comparison of its performance against the operational Western North Atlantic (WNA) wave model during hurricanes Isidore and Lili, in 2002, are presented. The NAH and WNA models are identical in their physics and numerics. However, the NAH model uses a wind field obtained by blending data from NCEP's operational global weather forecast system (GFS) with those from a higher resolution hurricane prediction model, whereas the WNA wave model uses winds provided exclusively by the GFS. Relative biases of the order of 10% in the prediction of maximum wave heights up to 48h in advance, indicate that the use of higher resolution winds in the NAH model provides a successful framework for predicting extremes sea states generated by a hurricane. Consequently, the NAH model has been made operational at NCEP for use during the Atlantic hurricane season.

Acknowledgments.We thank Timothy P. Manchok, Morris Bender and Robert E. Tuleya, of NOAA's Geophysical Fluid Dynamics Laboratory, for providing valuable information regarding the GFDL hurricane model and providing input data for our hurricane wave model. We also acknowledge the valuable support, observational wave data and wind analysis products provided by NOAA's National Data Buoy Center (NOAA/NDBC) and Hurricane Research Division (NOAA/HRD).

This report is available as a pdf file from

http://polar.ncep.noaa.gov/waves

Contents

This page is intentionally left blank.

1 Introduction

Improving the skill of operational forecasts of wind-wave fields associated with hurricanes has received much attention in recent years. This effort is justified by the damage to coastal settlements and economic activities in coastal and offshore regions associated with the occurrence of extreme waves generated during intense hurricanes. This trend has been followed at the National Centers for Environmental Prediction (NCEP), where presently two hurricane wave models provide regional wave forecasts in the north Atlantic and Pacific ocean basins.

The North Atlantic Hurricane (NAH) and North Pacific Hurricane (NPH) wave models are part of the NOAA WAVEWATCH III wave forecasting system, which also includes a global model (NWW3), and three other regional models covering the following domains: Alaska Waters (AKW), Western North Atlantic (WNA) and Eastern North Pacific (ENP). All models in the NWW3 suite are implementations of the third-generation spectral ocean wave model WAVEWATCH III (Tolman and Chalikov, 1996; Tolman, 1991, 2002; Tolman et al., 2002). A detailed description of the NWW3 wave forecasting system and of some of its applications may be found in Chao et al. (1999a,b), Chao et al. (2001) and Tolman et al. (2002). All wave models in the NWW3 system are driven with wind forecasts from NCEP's Global Forecast System, GFS (Moorthi et al, 2001), previously known as MRF/AVN, (Kanamitsu et al. 1991; Caplan et al. 1997). Hurricane models are driven with GFS winds blended with higher resolution winds, as will be described below.

It is well known that the details of intense and rapidly varying wind fields associated with tropical cyclones are poorly resolved by general atmospheric circulation models such as the GFS. The main reasons for this are that the intrinsic spatial and temporal resolutions of global models are usually too coarse to resolve the wind field structure associated with a relatively small hurricane vortex (Surgi et al., 1998; Chao et al., 2001). For the GFS model, the spatial resolution is of the order of 50 km in latitude-longitude, while wind fields are made available for the wave models at 3h intervals. As a result, predicted wave heights in areas under the influence of tropical storms are usually unrealistically low or are predicted over an area that is too large.

In order to provide more accurate forecasts of storm tracks and wind intensities, NCEP uses a separate atmospheric model during hurricane seasons, providing additional forecast guidance for NOAA's National Hurricane Center (NHC). This model, developed at the Geophysical Fluid Dynamics Laboratory (GFDL), is a multiply nested, movable mesh model involving variable grid resolutions as described in detail by Kurihara et al. (1980, 1990, 1995, 1998). At NCEP, the GFDL model is implemented with two nested movable grids consisting of a finer inner mesh centered at the hurricane and an outer coarse mesh (see below). This implies that the GFDL model can only target one storm at a time. When multiple

storms exist simultaneously, a single targeted storm is centered in the inner grid, while other storms appear in the coarse outer mesh. The details of wind fields associated with storms in the outer mesh again may be not adequately described.

Since only one storm can be tracked per GFDL model run, the combined effects of various wind fields from co-existing storms on generating wind waves cannot be adequately predicted using the output of a single GFDL model run. However, when multiple storms co-exist, independent GFDL model runs are made at NCEP targeting each storm individually. From the perspective of wave modeling, this introduces two problems. First, no single forecast product is available with optimal high resolution wind fields for all hurricanes. This is a key issue for simulating hurricane wave fields from multiple storms because swell systems generated by individual systems propagate far away from the generating storm. Second, often the GFDL grids do not cover the entire wave model domain, which is fixed.

The solution to these problems is to blend higher resolution GFDL winds within the area of influence of each hurricane with GFS winds in the far field, thus providing a single wind field covering the entire wave model domain. Both the NAH and NPH wave models incorporate such a procedure for an arbitrary number of hurricanes (Chao and Tolman 2000, 2001). The NAH model, the main focus of the present study, has been operational since June 2001. Its domain extends from 98° W to 30° W and from the equator to 50° N. This domain is identical to that of the Western North Atlantic (WNA) regional wave model, which has been operational since March 2000. The fundamental difference between the WNA and NAH models is that the former is driven exclusively with GFS winds, while the latter is forced with blended GFDL and GFS winds, as described above.

It should be noted that under the operational scheduling of NCEP's central computing system (CCS), the WNA model is run at the same time as GFDL runs are being made and directly after a full GFS model cycle is concluded. The NAH model can only be initiated after all GFDL runs are concluded. Therefore, operational products generated by the WNA model are available much earlier than products from the NAH model. This is the main reason for keeping both models running operationally, instead of replacing the WNA model with the NAH model.

In this paper we review the development of the NAH wave model and investigate in more detail its performance during the 2002 hurricane season. Our performance assessment of NAH is made relative to wave forecasts generated by the WNA model. We present the results of our investigation as follows. We describe in Section 2 the procedure for blending GFS and GFDL model winds. In Section 3, we describe the methodology used to forecast hurricane waves using blended wind fields. Section 4 summarizes previous results obtained during the development and testing stages of the NAH wave model. The validation of predicted winds and waves against buoy measurements is presented in Sections

5 and 6. We provide a discussion focusing on results, limitations and outlook for future improvements to the NCEP hurricane wave forecasting models in Section 7. Finally, our concluding remarks are presented in Section 8.

This page is intentionally left blank.

2 Wind field specification for hurricane wave models

The GFS atmospheric model currently operational at NCEP (Moorthi et al, 2001) provides basic wind information for the WNA and NAH models, as well as for all other wave models under the NWW3 system. The GFS model runs 4 cycles per day at 00Z, 06Z, 12Z and 18Z. It generates global forecasts at 3h intervals up to 180h, and at lower spatial and temporal resolution up to 16 days. The present operational GFDL hurricane model also runs 4 cycles per day at 00Z, 06Z, 12Z and 18Z. Regular outputs of the GFDL model to the general public are made at 6h intervals up to 126h. A separate dataset consisting of hourly sea level pressure and wind fields at GFDL's lowest layer (about 35m from the surface) up to 72 hours is specially generated for use in wave forecasts.

Since the initial period of development and testing of the NAH model (see below), the GFDL model has undergone substantial modifications. The first version of the GFDL model used to drive the NAH wave model had three spatial grids with horizontal resolutions ranging from 1° to 1/3° to 1/6° covering an area of 75° x 75° , 11° x 11° and 5° x 5° in latitude-longitude, respectively (Kurihara et al., 1998). Modifications incorporated since then and up to the year 2002 hurricane season included improvements in hurricane initialization (Liu et al., 2000), the implementation of a hurricane-ocean coupling kernel (Bender et al., 2001) and the implementation of the current two-nested-grid configuration (Bender, et al., 2002).

Since the 2002 hurricane season and up to the present, data from NCEP's GFDL model have been provided at two grid resolutions. The coarse grid has uniform 1/3° resolution covering an area of 75° x 75° in latitude-longitude. The inner, finer nested mesh has a uniform 1/6° grid resolution covering an area of 11° x 11° in latitude-longitude. At any given time step, the center of the finer mesh is aligned to a single storm center and, therefore, moves with the storm as it propagates. The outer, coarse grid has fixed north and south boundaries at 65° N and 10° S, but moves freely on the west-east axis following the storm center.

Since an individual GFDL hurricane model run can only target a single storm, several runs are needed when more than one storm exists. Thus, discrepancies in the wind field features for the same storm but from different GFDL model runs may occur. Furthermore, the storm center and extent of wind field forecast by GFDL and GFS may also have discrepancies. In order to obtain a single representative description of each system, the concept of area of influence (AOI) for each storm is introduced.

Various definitions of AOIs have been considered and tested, resulting in the following procedure used to determine the wind field structure for hurricane wave prediction within the NWW3 wave prediction system:

(a) Construct the underlying 10-meter height wind fields on a regular latitude-longitude grid at 0.5° resolution from the lowest σ-level outputs generated by the GFS model, assuming neutral atmospheric stratification.

(b) Interpolate 10-meter height GFS winds from 3-hour intervals to hourly intervals and to the NAH grid at a 0.25° resolution.

(c) Interpolate the hourly GFDL mean sea level pressure field and the lowest layer wind on coarse and fine grids to the wave model grid resolution and adjust winds to 10-meter height, assuming neutral atmospheric stratification.

(d) Locate the hurricane eye (lowest sea level pressure) based on the GFDL model mean sea level pressure field.

(e) From the storm center, determine a box area extending outwards to the north, south, east and west until its sides intersect the 1015mb isobar, using the GFDL model surface pressure field.

(f) Determine a second box area extending from the hurricane eye to where the wind speed decreases to 7.5 m/s or less on each side of the box, based on the GFDL wind field.

(g) Similarly, based on the GFS wind field determine a third box area extending from the hurricane center to where the wind speed decreases to 7.5 m/s or less on each side of the box.

(h) Form a new box area with sides defined as the largest distance to the hurricane eye among the sides of the three boxes defined in (e), (f) and (g).

(i) Restrict box sides to be at angular distances less or equal to 12.5° and greater or equal to 3.5° from the hurricane eye in case the box defined in (h) violates this criterion.

The area so specified is assumed to be the AOI of any given storm. GFS winds within each AOI are replaced with GFDL winds. To warrant a smooth transition from GFDL winds inside each AOI to GFS winds in the outer storm domains, a weighted average procedure using linear coefficients is employed within bands with a fixed width of five model grid points (i.e., 1.25°) surrounding the AOI. A similar procedure is employed when two or more AOIs overlap. For more details about the procedure outlined above, see Chao and Tolman (2001b).

An example that shows the resulting blended wind field constructed using the procedure described above is illustrated in Figure 1 for the 12Z cycle forecast on September 25, 2002 when three hurricanes coexisted. These were hurricanes Isidore, Kyle and Lili. Figure 1(c) shows the wind field over the wave model

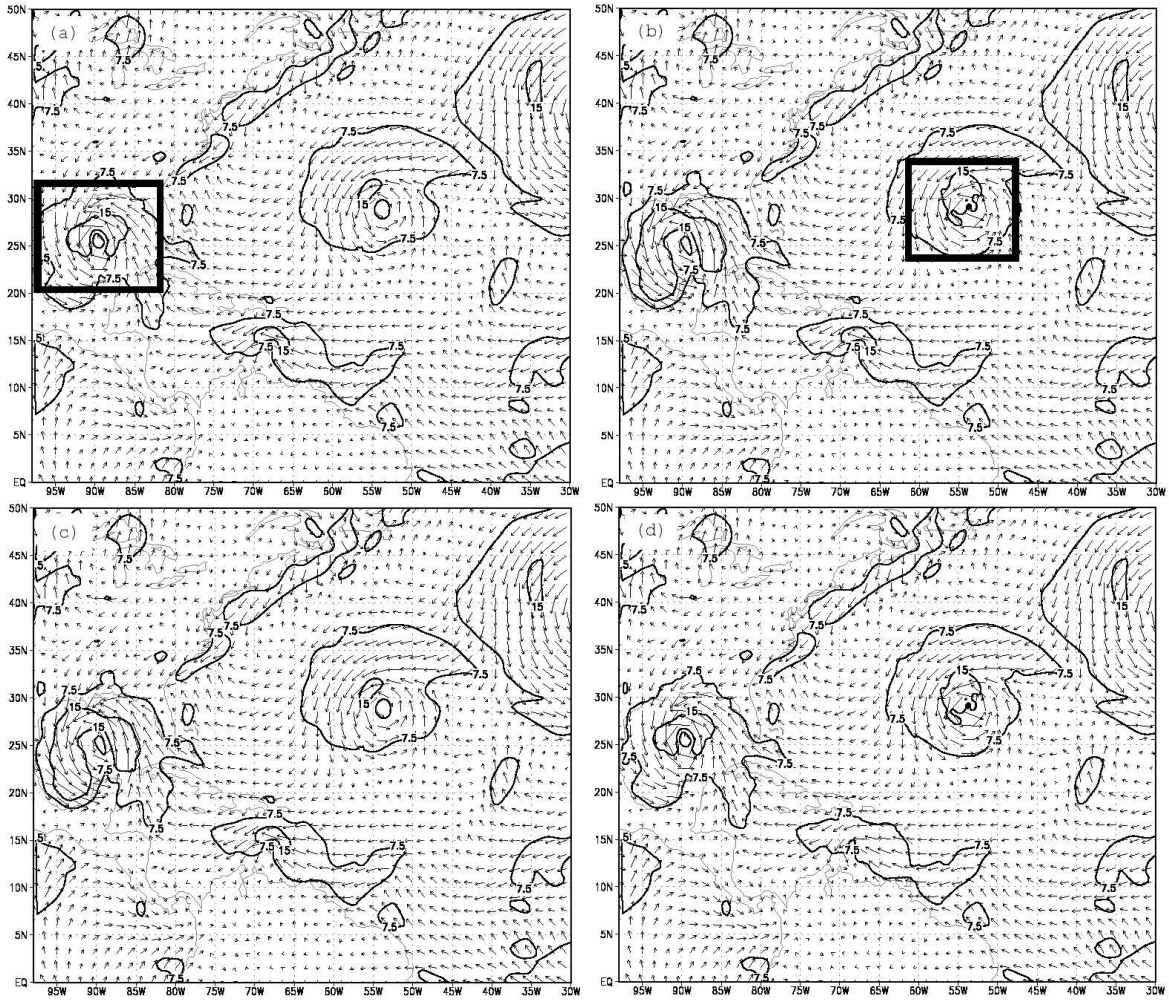

Figure 1: Sources of wind fields used for driving the NAH model on September 25th 2002 at 12h UTC. Individual fields are shown for (a) GFDL winds for hurricane Isidore, (b) GFDL winds for hurricane Kyle, (c) GFS winds only and (d) blended GFS and GFDL winds using data for Isidore, Kyle and Lili (the latter is not shown individually).

domain obtained based on GFS forecast. Hurricanes Isidore, Kyle and Lili are located in the Gulf of Mexico, the middle Atlantic Ocean and in the eastern Caribbean Sea, respectively. The boxes in Figure 1(a) and (b) represent the wind fields taken from GFDL model runs specifically for hurricanes Isidore and Kyle, respectively, blended individually with the GFS forecast field. Figure 1(d) shows the final wind field used in the wave model, which consisted of GFDL winds from each of the three hurricanes combined and blended with GFS winds.

It should be noted that the GFDL forecasts of Isidore in Figure 1(a) are relatively weaker than the GFS forecast in Figure 1(c), while GFDL winds for Kyle in Figure 1(b) are stronger. Furthermore, the patterns of wind fields from the GFDL model runs specifically for Hurricane Kyle, shown in Figure 1(b), differs from those shown in Figure 1(a). This is also true for the hurricanes other than the one targeted in a particular GFDL run. Therefore, only the final blended wind fields provide a consistent picture of all systems.

This page is intentionally left blank.

3 Procedure for predicting hurricane waves

The Atlantic hurricane season formally runs from June 1st to December 1st. On the NWW3 web site[1], NAH model results are displayed only within this time window unless a tropical storm is identified (e.g., hurricanes Odette and Peter, between December 4th and 11th 2003). For practical reasons, however, the NAH model is run all year-round by NCEP Central Operations (NCO). The NAH model is kept running even when no GFDL winds are available, to ensure proper tracking of swell systems generated by pre-existing hurricanes even when the system has long ceased to exist. In such conditions, the WNA and NAH models share identical surface winds fields, provided by the GFS model.

When output fields from GFDL model runs (i.e., mean sea level pressure and surface winds) are available, the procedure for wind field specification previously described is initiated. The resulting blended surface wind fields are used to force the NAH wave model, while boundary wave conditions at the edges of the NAH model domain are defined as in all other regional wave models at NCEP, i.e. from two-dimensional wave spectra produced by the global wave model NWW3.

Like all other models that comprise the NWW3 wave model suite, the NAH model runs four times per day at the 00 UTC, 06 UTC, 12 UTC and 18 UTC cycles. However, unlike most other models, NAH (and NPH) forecasts extend only out to 72-hours, because this is the current time window for availability of hourly data from GFDL model runs[2]. In all domains covered by the NWW3 system, each model cycle run includes a six-hour wave hindcast that precedes the actual forecasts. Wave hindcasts in models driven exclusively with GFS winds (Global, AKW, WNA and ENP) are generated using three-hourly analyses from GFS's Global Data Assimilation System (GDAS) for a 6-hour period preceding the current cycle's UTC time stamp. Unlike the GFS, the GFDL model does not include a system that assimilates observations for generating analysis fields prior to each model cycle. Therefore, the NAH wave model hindcasts are generated using the GFS analysis winds blended with GFDL winds for the 0h through 4h range from the previous cycle (-6h to -2h range in the current cycle). Wind data at the -1h time of the current cycle are obtained by interpolating the -2h winds with the blended GFS/GFDL 0h wind nowcast. This guarantees a smooth transition between short term forecasts and the ensuing analysis.

[1] see http://polar.ncep.noaa.gov/waves/

[2] This limit has been extended to 126h during the 2004 hurricane season

This page is intentionally left blank.

4 Model development and testing

The first version of the NAH wave model was implemented for the 2000 Atlantic hurricane season. This earlier model implementation proved the concept that more accurate hurricane wave forecasts required a specialized model implementation using higher resolution winds. In this section we provide a brief summary of major findings and improvements made during the first two years of operation of the NAH model. A more detailed evaluation of this development and testing phase is provided in Chao and Tolman (2000, 2001a). These papers, which were the basis for the development of the current hurricane wave model implementations at NCEP, report the performance of the NAH model using four case studies: hurricanes Floyd and Gert (1999 season) and Gordon and Helene (2000 season).

Results from Chao and Tolman (2000, 2001a) indicate that for intense hurricanes poorly resolved by the GFS model, more realistic GFDL winds typically resulted in more intense wave conditions. However, some cases were found in which the GFS model correctly predicted the intensity of relatively weak and small systems, but overestimated its spatial extend. Consequently, the WNA model overestimated wave conditions, whereas the NAH correctly predicted lower wave heights. Hence, it was found that for hurricane wave predictions it was not sufficient to simply increase the intensity of under-resolved systems. Instead, a generally better depiction of these small-scale features in the high-resolution GFDL model proved to be critical, justifying the approach of blended wind fields, instead of, for instance, using statistically enhanced wind fields such as the bias correction procedure described in Tolman (1998).

The first two years of NAH model operation also revealed some shortcomings of the initial model configuration. For practical reasons, we initially had access to GFDL wind fields at 6 hour intervals only. This resulted in problems with the interpolation in time of wind fields for fast moving systems. This problem became particularly obvious for hurricane Michelle in 2001, as shown by Chao and Tolman (2001b). To mitigate this problem, acces to NCEP's GFDL model hourly surface wind field outputs was provided specifically for the wave model. Positive impacts of these changes to hurricane wave forecasting are also described in Chao and Tolman (2001b).

Another important change implemented during the development and testing phase of the NAH model was a modification to the AOI scheme, to enssure that the GFS representation of each hurricane is properly replaced (covered) by the AOI. A detailed description of this procedure is provided in Section 3 above. This more mature version of the NAH model was implemented for the 2002 hurricane season and is the focus of the present study. This version was also the basis for the NPH model implementation in 2003.

This page is intentionally left blank.

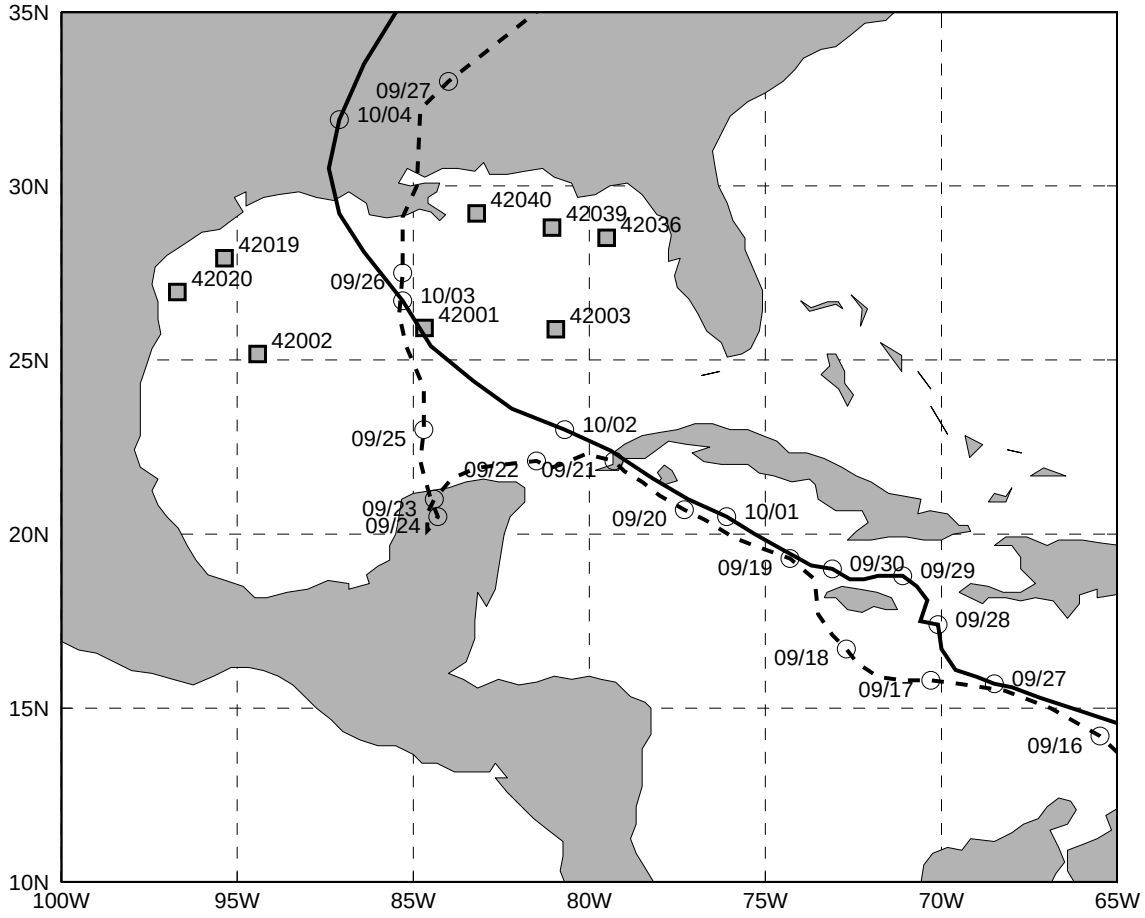

Figure 2: Location of selected NDBC/NOAA buoys. Best tracks for hurricanes Isidore (dashed line) and Lili (solid line) are also show. Daily 0h UTC positions are also indicated.

5 Selected events from the 2002 hurricane season

During the hurricane season of 2002, most storms were either far from the east coast of the USA or were not strong enough to generate severe wave conditions near the NDBC buoy network in the North Atlantic ocean. Two hurricanes, however, had a devastating impact in the Gulf of Mexico, occurring within less than a week from each other between September 18th and October 7th. Due to their strength and the extreme wave conditions observed in that period, these hurricanes, named Isidore and Lili, will be the focus of our validation study. Our validation strategy is based on a comparative assessment of the WNA and NAH model performances, using as a reference NDBC buoy observations. Model performance is evaluated in terms of hindcasts and height (H_s) and the peak

wave period (T_p). Validation is performed against wave parameters recorded at eight NDBC/NOAA buoys deployed in intermediate and deep waters within the Gulf of Mexico. Figure 2 shows tracks of hurricanes Isidore and Lili, along with the locations of the eight NDBC buoys used presently. The main characteristics of the NDBC buoys are given in Table 1.

WMO Code	Location	Position		Depth (m)
		Longitude	Latitude	
42001	Mid-Gulf of Mexico	89.68W	25.92N	3,246
42002	West Gulf of Mexico	94.42W	25.17N	3,200
42003	East Gulf of Mexico	85.95W	25.88N	3,164
42039	Pensacola, FL	86.06W	28.80N	283.5
42040	Mobile South, AL	88.20W	29.21N	237.7
42019	Freeport, TX	95.36W	27.92N	82.3
42020	Corpus Christi, TX	96.70W	26.95N	78.6
42036	West Tampa, FL	84.51W	28.51N	53.0

Table 1: NDBC buoy locations, World Meteorological Organization (WMO) codes, geographical positions and water column depth.

5.1 General Characteristics of Hurricanes Isidore and Lili

Hurricane Isidore evolved from a succession of westward moving tropical depressions near Jamaica, becoming a hurricane on 09/19/02, at 0800 UTC. On September 21st it entered the Gulf of Mexico, after sweeping the northwestern edge of Cuba and veering westward toward the Yucatan Peninsula, with winds over 110 kn (57 m/s). After its first landfall, Isidore meandered over land and re-entered the Gulf of Mexico moving northward as a tropical storm, until making landfall west of Grand Isle, Louisiana on Sep 26th at 6 UTC.

A tropical depression originated in the tropical Atlantic Ocean became hurricane Lili on September 30th. In the morning of October 1st it passed over western Cuba and entered the Gulf of Mexico, with wind speeds as high as 90 kn. The hurricane moved with advection speed around 15 kn in a nearly straight northwesterly path. Lili made landfall on the Louisiana coast on October 3rd with an estimated 80 kn maximum wind speed, leaving behind 13 deaths and damages over US$ 860 million. A detailed anaysis of Isidore and Lili are provided in Avila (2002) and Lawrence (2002), respectively.

5.2 Synoptic Patterns of U_{10}, H_s and T_p

It is constructive to present a qualitative description of model analysis and predictions of wind and wave patterns to examine model performance in general

and provide useful information for the interpretation of observed conditions to be given in the next section.

Hurricane Isidore

Due to the intense momentum transfer induced by storm winds to the ocean surface, high-energy swell is rapidly generated by hurricanes. As they radiate from the hurricane's maximum wind region, these swell fields soon outrun the storm and become dominant relative to surrounding background wave fields, forming a front-like pattern that is easily identified due to the strong contrast to pre-existing waves. In this manner, swell generated by hurricanes or other systems with strong wind fields become forerunners of storms, as first pointed out by Munk (1947). During Isidore's passage over the Gulf, swell forerunners were generated even before the hurricane's eye entered the Gulf of Mexico by a massive band of strong winds developing north of Cuba. Surface winds and T_p fields from the NAH model outputs at selected time stamps highlighting the propagation of swell fronts are shown in Figure 3(a,b). In the figure, Isidore's eye was still south of Cuba (Figure 2).

After crossing the Yucatan channel between Mexico and Cuba and making landfall at the Yucatan Peninsula, Isidore re-entered the Gulf and followed a northward track, before making its final landfall in the Louisiana coast. During this stage, Isidore actively generated local waves within its maximum wind region, which superposed onto swell generated during its previous westward-track passage between Cuba and the Mexican coast, particularly along the western Gulf coast. Theses swell systems were, at the same time, being superposed by local waves generated by intense southward winds near the coast associated with Isidore's western sector. This complexity of superposing wave systems and associated winds is illustrated in Fig. 3(c,d).

Hurricane Lili

Model predicted surface wind and wave fields associated with the passage of Lili over the Gulf are shown in Figure 4. Lili's rather straightforward trajectory generated maximum H_s fields that closely followed the maximum wind path, as can be seen in Figure 4 (also on the bottom right in Figure 3c and d). Nevertheless, the H_s patterns also indicate that the hurricane generated swell forerunners with noticeable energy propagating westward and northward, radiating from the hurricane track. The generation of swell forerunners, which became the dominant waves in a large area within the Gulf is confirmed by the spatial distribution of T_p shown in Figure 4(c,d). Soon after Lili's entrance into the Gulf, a radial front of dominant waves with periods as low as 12 s became dominant in a large area of the Gulf. As the hurricane continued moving northwestward the fan of swell

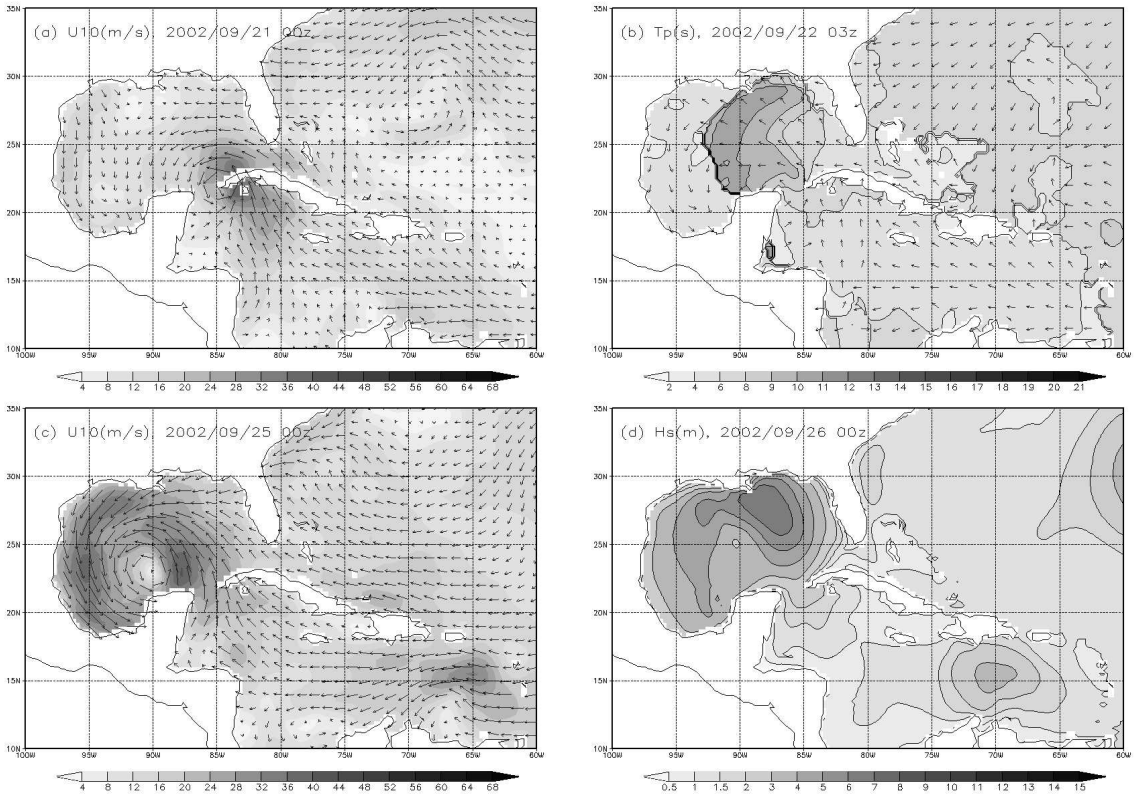

Figure 3: Wind and wave fields from the NAH model during hurricane Isidore: (a) U_{10} on September 21st 0h UTC and (b) T_p indicating resulting swell fields on September 22nd 3h UTC; (c) U_{10} on September 25th 0h UTC and (d) associated H_s on September 26th 0h UTC.

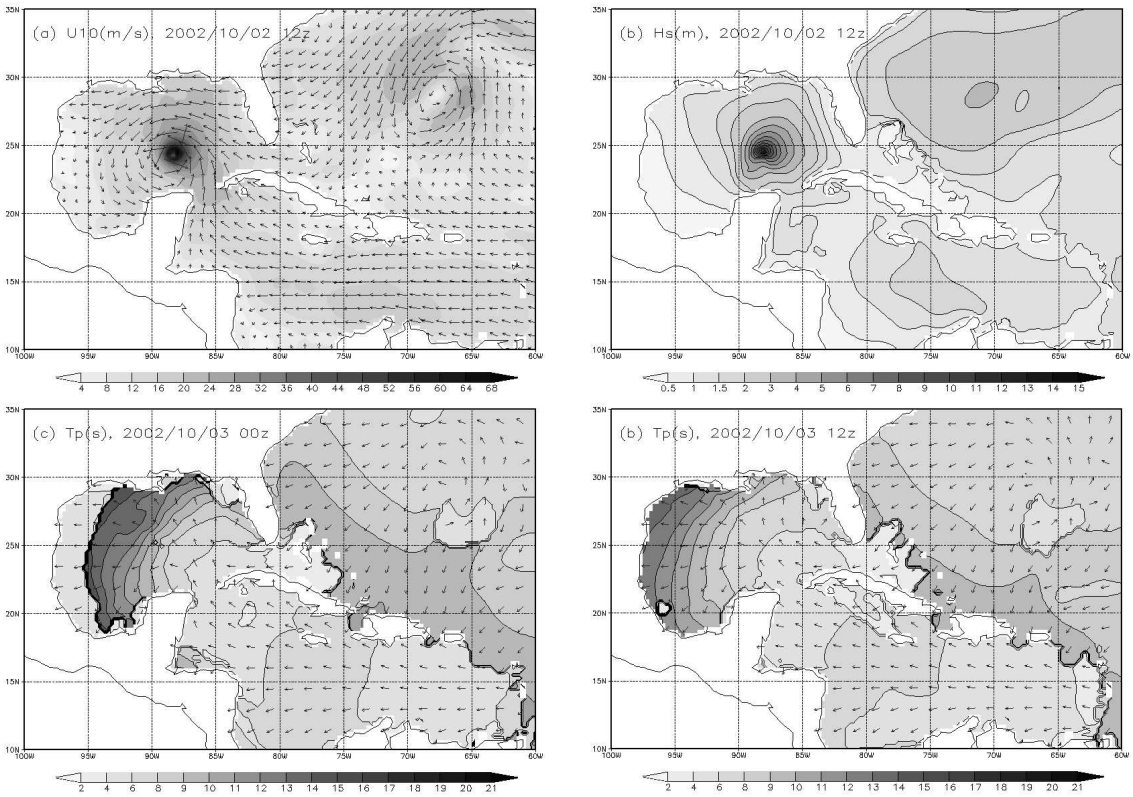

Figure 4: Wind and wave fields from the NAH model during hurricane Lili: (a) U_{10} and (b) H_s showing the hurricane at its maximum strength on October 2nd 12h UTC; (c) and (d), dominance of swell fields throughout the Gulf of Mexico on October 1st 0h and 12h UTC, respectively.

forerunners widened its area of coverage, sweeping an area spanning from the western coast of Florida to the western reaches of the Campeche Bank in Mexico. These swell fields are shown in Figure 4(d) reaching the eastern coast of Mexico and southern shores of Texas, after the hurricane made landfall on the Louisiana coast.

5.3 Time Series of U_{10}, H_s and T_p

Figures 5, 6, and 7 show time series of U_{10}, H_s and T_p, respectively. These figures compare measurements at eight NDBC buoys with the results of NAH and WNA model predictions. Model data were generated via interpolation to the buoy location of outputs from surrounding grid points. The listing hierarchy used in these figures from top to bottom, show deeper to shallower water buoy locations as given in Table 1. The first three buoys (42001, 42002, and 42003) are deployed in the deep Gulf region, whereas the remaining buoys are distributed along the

western (42019 and 42020) and eastern (42036, 42039 and 42040) coastal regions of the Gulf.

Hurricane Isidore

None of the NDBC buoys were directly under the hurricane path during the first passage of Isidore over Gulf waters between Cuba and Mexico. Isidore's existence was recorded as a small peak around September 22nd in measurements of U_{10} at buoy 42003, the closest to the hurricane's maximum wind region, as seen in Figure 5(c). On the other hand, wind fields associated with Isidore during its second stage directly affected most buoys. Buoys located to the east of the storm track during its second stage (42001, 42003, 42036, 42039 and 42040) were all near the maximum wind region at some time. Wind intensities recorded at these locations had typically one distinctive peak in the time series of U_{10} shown in Figure 5, starting on September 25th (buoy 42001) and extending up to September 27 (buoy 42040). Time series of U_{10} recorded at buoys to the west of Isidore's path were characterized by a 'plateau' near U_{10}=12 m/s during the storm's second stage between September 23 and 27, as seen in Figure 5. This plateau reflects the widening of Isidore's western wind sector as it transitioned from a hurricane to a tropical storm, which produced a large band of strong northerly winds extending over buoys 42002,42019 and 42020.

Isidore generated wave fields that superposed in a complex manner throughout its lifetime, as a consequence of its peculiar, L-shaped track. During Isidore's first stage, only buoy 42003 recorded a clearly distinguishable signal possibly associated with local wind seas generated at the hurricane's maximum wind region. This is reflected by the increasingly high wave heights H_s recorded between September 20th and 23rd, as shown in Figure 6 (c). Associated values of T_p during this period, shown in Figure 7 (c), increased from 6 s to 11 s. Although a similar but weaker pattern is also seen in H_s recorded at buoy 42001 in Figure6 (a), values of T_p shown in Figure 7 (a) suggest a predominance of swell forerunners over local wind seas at this location. Waves generated by Isidore during its first stage were barely noticeable in H_s recorded at buoys 42036, 42039 and 42040, all located away from the direct influence of hurricane force winds, as shown in Figure 6 (d, e, h). Despite the low wave heights, the arrival of swell generated by the hurricane appears as a clear signal in the recorded series for T_p in Figure 7 (d, e, h) as intermittent jumps from around 6 up to 12 s between September 22nd and 24th.

Buoys 42002, 42019 and 42020 recorded a more complex superposition and sequence of wave field patterns. The first waves to arrive at these locations were swell systems generated during the westward advection of hurricane Isidore between Cuba and Yucatan. Their arrival caused a sudden increase in the values of T_p between September 23rd and 26th, as shown in Figure 7(b, f, g). This was

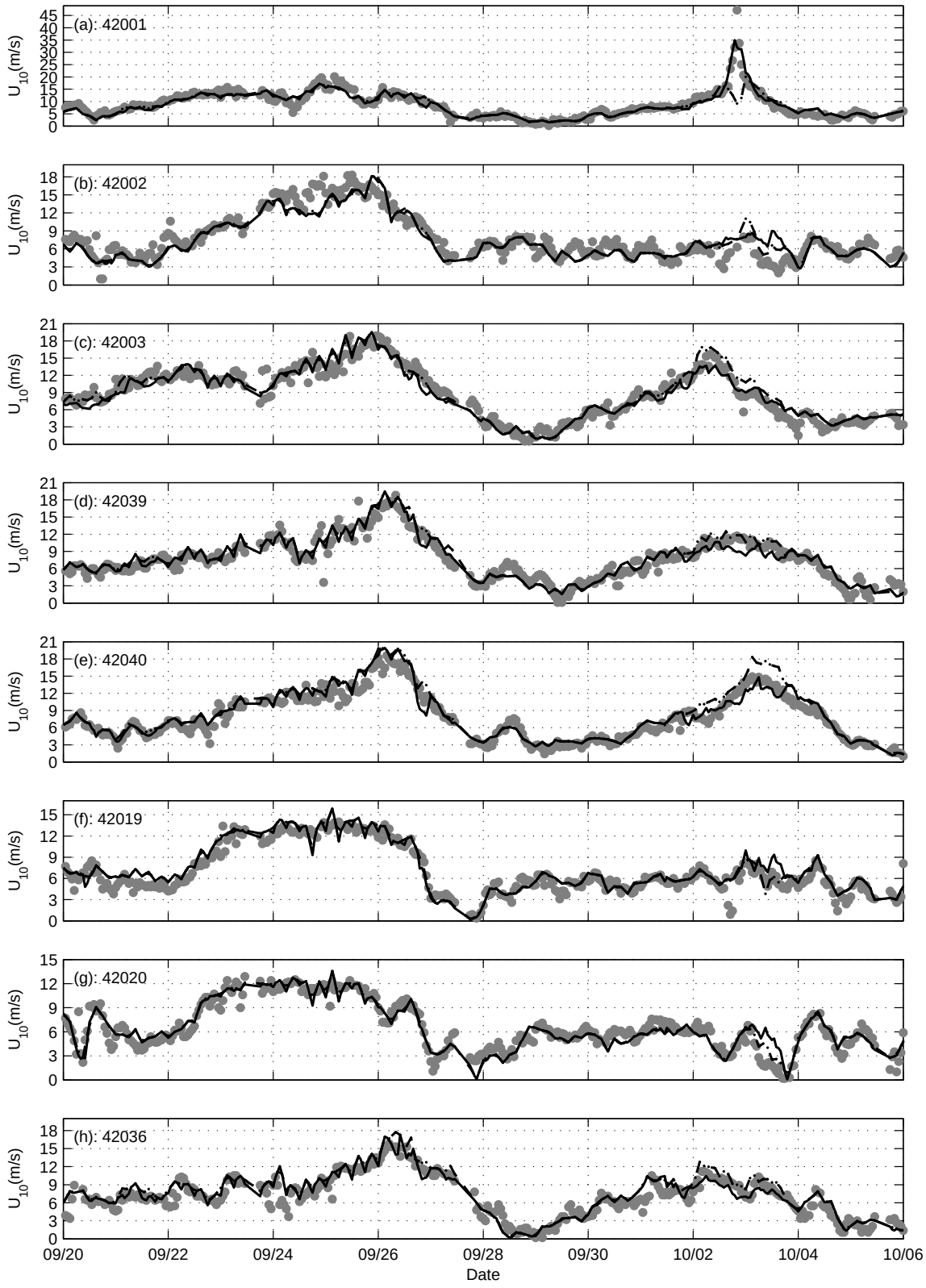

Figure 5: Time series of U_{10} at selected NDBC/NOAA buoy locations. Hindcast data from the WNA (dashed line) and NAH (solid line) models are compared to Observations (gray circles).

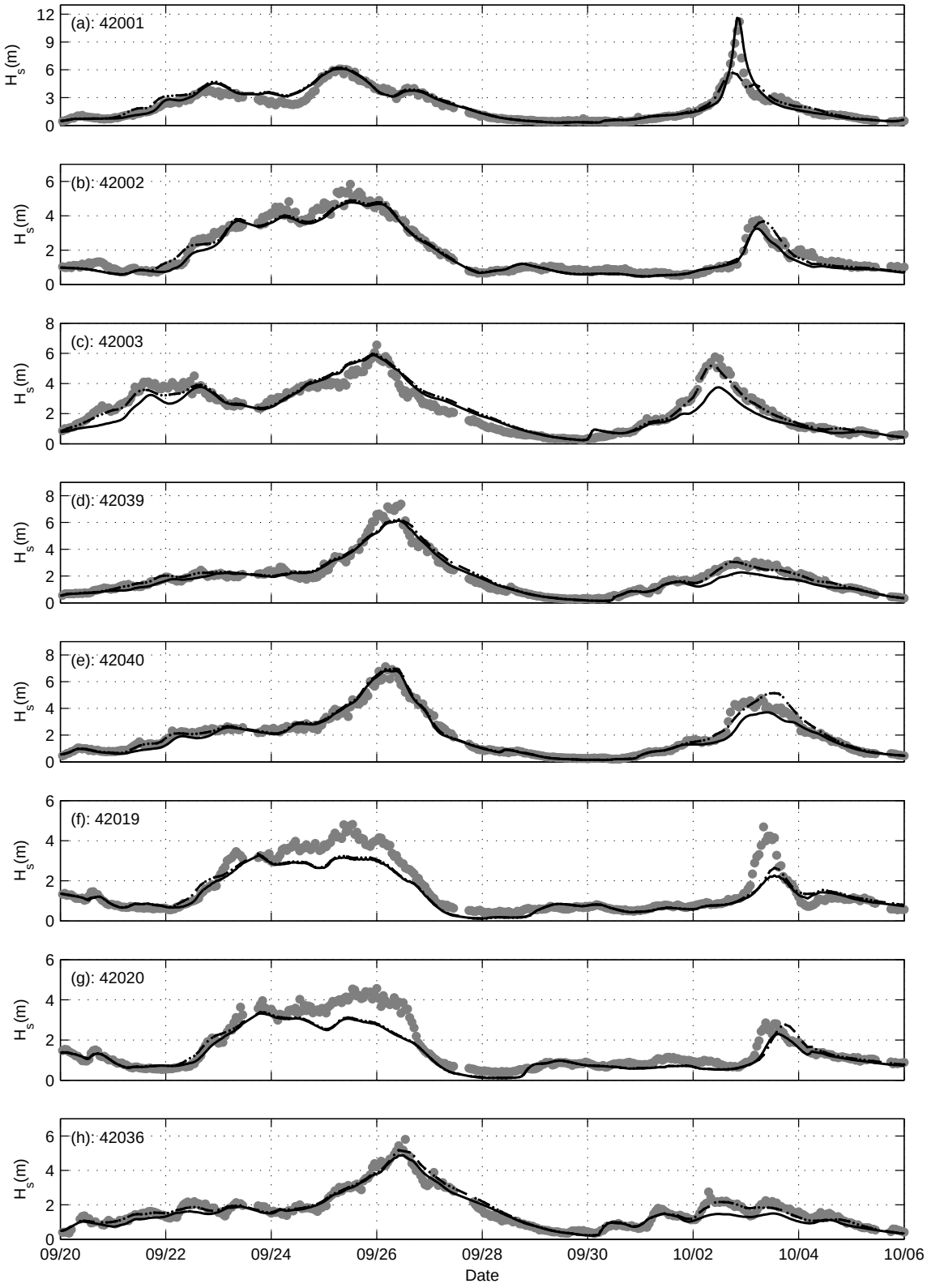

Figure 6: Time series of H_s at selected NDBC/NOAA buoy locations. Hindcast data from the WNA (dashed line) and NAH (solid line) models are compared to Observations (gray circles).

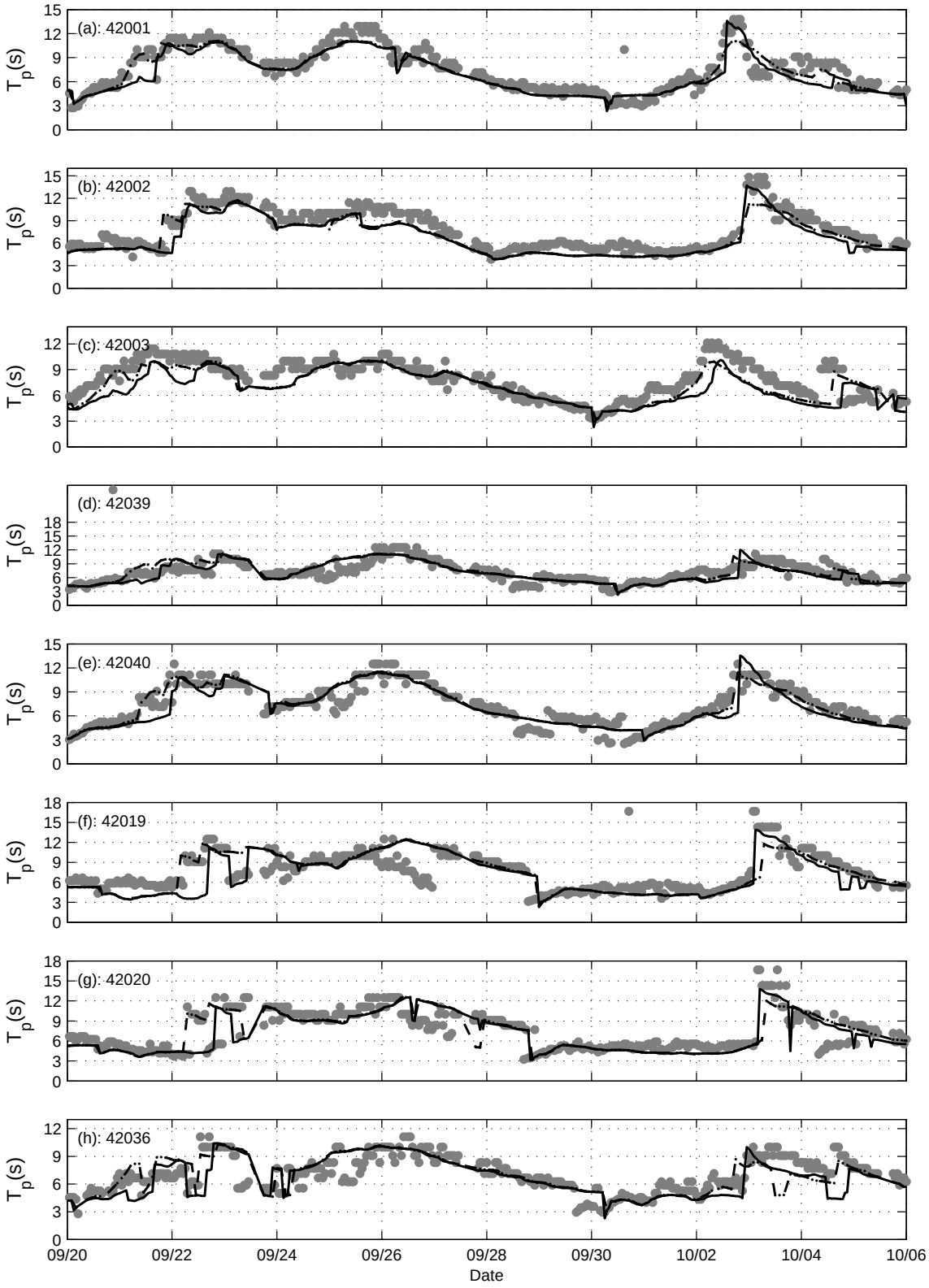

Figure 7: ime series of T_p at selected NDBC/NOAA buoy locations. Hindcast data from the WNA (dashed line) and NAH (solid line) models are compared to Observations (gray circles).

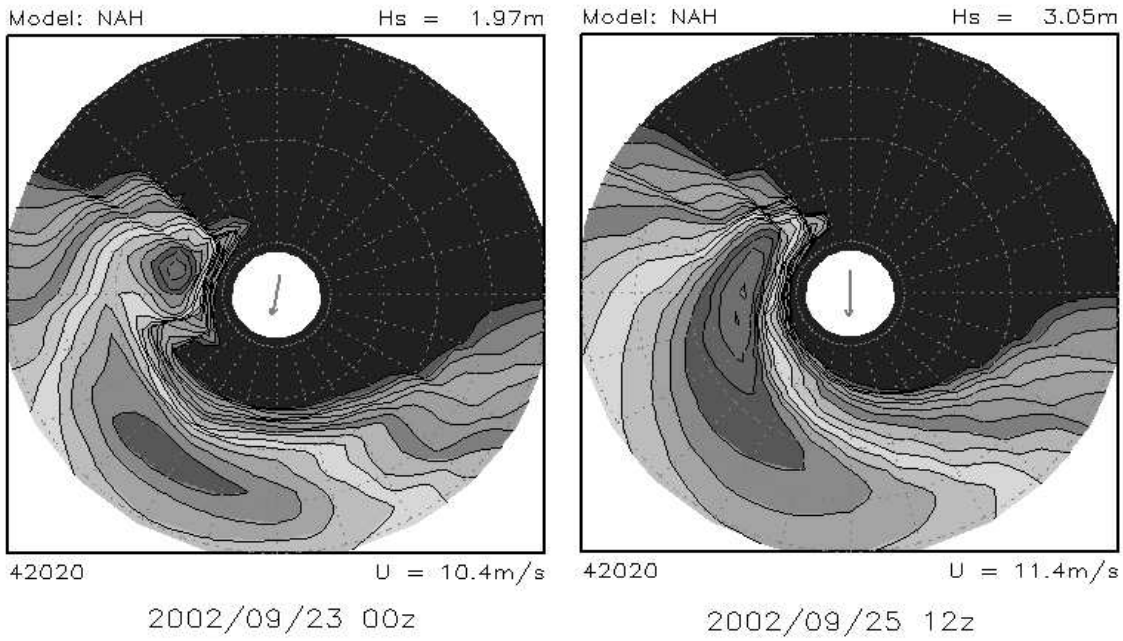

Figure 8: NAH model output spectra at NDBC buoy 42020 (corpus Christi, TX) illustrating the superposition of westerly swell generated by Isidore's early stages with local northeasterly windseas on September 23rd (left). The right panel shows the superposition of westerly swell and local windseas associated with Isidore on September 25th.

followed by a gradual increase in H_s (see Figure 6). Due to the large distance between these buoys and the swell sources, their gradual arrival was mixed with the occurrence of wind seas generated locally by the strong northwesterly wind in the western Gulf region during the northward movement of Isidore [Figure 3(c)] during its second stage. This superposition of swells and local wind seas can be seen in two-dimensional model spectra as illustrated in Figure 8. Model spectra at western buoys also suggest the presence of easterly swell generated by Isidore's maximum wind region during its second stage, as shown in Figure 8(b).

A further illustration of the progressive superposition of swell waves recorded at buoys located to the west of Isidore's track is shown in Figure 9(a). This figure consists of a diagram showing the time series of one-dimensional frequency spectra recorded at buoy 42020, in which the dispersive arrival of swell events appears as "ridges" formed by energy density level contours that shape around progressively decreasing values of peak frequency f_p in consecutive spectra. Such spectral peak ridges develop as a consequence of longer period (lower frequency) swell fields generated by distant storms arriving earlier than swells with shorter periods (higher frequencies) due to dispersion. Average ridge lines drawn in

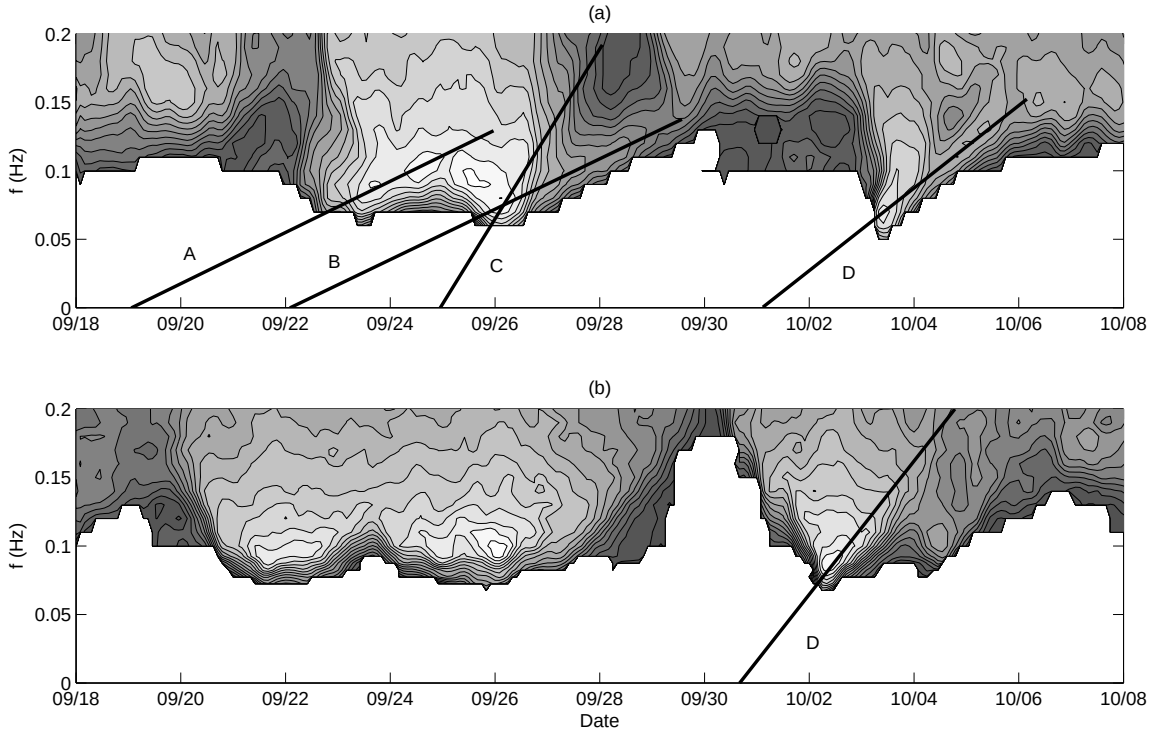

Figure 9: Time series of one-dimensional frequency spectra (Munk-Barber-Ursell diagram) measured at NDBC buoys (a) 42020 and (b) 42003. In these diagrams the horizontal and vertical axes show time and frequency, respectively.

Figure 9(a) through peak periods associated with individual ridges identify the three more conspicuous swell events during Isidore up to around September 28. Generation times and distances traveled by each swell system were determined from the slope and intercept of ridge lines relative to the time axis (x), following the technique first devised by Barber and Ursell (1948) and Snodgrass et al. (1966).

The ridges in Figure 9(a) indicate that the first swell systems to arrive at the western buoys, around September 23, were generated just before Isidore's eye entered the Gulf, on September 19th. At this stage, the storm's northern sector winds were already over Gulf waters with enough intensity to have generated wave fields that evolved into this first swell event, as seen in Figure 3(a). The two subsequent swell events indicated in Figure 9(a) arrived almost simultaneously and immediately after the first swell event was fading. The 'older' of these two latter events was generated when the hurricane was in its first stage, moving westward between Cuba and Yucatan. It is represented by the less steep ridgeline intercepting the time line on September 22nd. The third swell event associated with Isidore was generated on September 25th, when the system had been down-

graded to tropical storm status and was moving northward. Recorded spectra shown in Figure 9(a), provides evidence that the plateaus seen in H_s recorded at western buoys between September 23rd and 26th [Figure 6(f,g)] result from the superposition of these swell systems with local wind seas.

Hurricane Lili

In contrast to hurricane Isidore, the passage of hurricane Lili generated a clear rise in wind intensities recorded at buoys located to the east of its track (42001,42003, 42039 and 42040), while time series of U_{10} from buoys to the west showed little indication of the hurricane's presence (42002,42019 and 42020), as shown in Figure 5. Waves generated during the passage of hurricane Lili over Gulf waters are seen as conspicuous peaks in the recorded time series of H_s and T_p at all buoy locations. Wave systems generated before Lili entered the Gulf propagated as swell forerunners and generated peaks in values of T_p at all buoys between October 2nd and 3rd. Wind seas generated within Lili's northwestward moving fetch produced a maximum H_s of 11.2 m recorded at buoy 42001 on the evening of October 2nd. This was the highest H_s value for the entire period among all buoy locations.

Lili's moving fetch also generated swell systems that were recorded as peaks in the time series of H_s at buoys 42002,42019 and 42020 on October 3rd. Figure 9(b) shows the time evolution of one-dimensional spectra measured at buoy 42003. The peak frequency ridge line shown in this figure illustrates the dispersive arrival of swell measured by buoys located to the east and west of Lili's track. In Figure 9(a), the swell ridge appears evolving centered at f_p=0.05 Hz and 0.15Hz between October 3rd and 5th. The swell ridge is also clearly separated from the spectral signature of local windseas generated by the hurricane, which appears as a slanted ridge with decreasing values of f_p ranging from 0.1Hz to 0.2Hz between October 3rd and 4th. In Figure 9(b), local windseas and swell ridges are hardly distinguishable, indicating a strong superposition of these two crossing wave systems. This is an expected situation since buoy 42003 was exposed more directly to Lili's maximum wind region and, thus, stronger windseas than buoy 42020, where the predominance of swell is more evident.

This page is intentionally left blank.

6 Validation of Model Predictions

The evaluation of model performance is made relative to NDBC buoy data. We start with a more general analysis of model performance in terms of standard validation statistics: bias (Bias), root-mean-square error (Erms), RMS-error scatter index (SI) and correlation (r). For a definition of these parameters, see Cardone et al. (1996). We then focus on investigating the model performance in terms of predicting the storm peak, represented through maximum or extreme wave heights, at each buoy location.

In all cases the assessment is made of both wave hindcasts and forecasts up to a 72h horizon. In this way, our performance assessment provides a comprehensive overview of WNA and NAH model performance during the passage of hurricanes Isidore and Lili through the Gulf of Mexico between September 26 and October 6, 2002.

6.1 Wind Analyses and Wave Hindcasts

Analyzed wind fields are usually the best available description of the state of the atmosphere during a given period of time in the recent past. Consequently, wave hindcast data obtained based on these wind input fields provide a good opportunity for assessing the skill of the wave model itself and of the quality of the nowcasts issued by the wave forecasting system. In the case of comparing the WNA and NAH wave models, this statement may be disputed since the quality of the hindcast wind input to NAH is somewhat different to that of hindcast winds driving the WNA model, as described previously.

The WNA model is driven exclusively by analysis winds computed with the aid of measured data assimilated into NCEP's GFS/GDAS, whereas the NAH wave model uses GFS/GDAS analyzes blended with GFDL *forecasts* from a previous model cycle (i.e., no analysis winds are available from GFDL runs). Although this may seemingly lead to lower quality winds available for the NAH model, the higher resolution winds available from the GFDL short-range forecast (0h-6h) may compensate for deficiencies in the lower resolution GFS/GDAS analyzes. This seems to be particularly true when hurricanes are present, as suggested by comparisons between pure GFS (WNA) and blended GFS/GFDL (NAH) winds with analysis wind fields provided by NOAA's HRD (see below). In any case, our performance assessment of wave hindcasts assumes that both WNA and NAH use the best available winds.

Table 2 represents bulk validation statistics of wind intensity U_{10} and wave field parameters H_s and T_p from the WNA and NAH wave models. The differences between the performance of the NAH and WNA models are relatively modest, with WNA slightly outperforming NAH at most buoys located away from the track of both hurricanes Isidore and Lili. This behavior was most pronounced at

Location	Model	U_{10}				H_s				T_p			
		Bias (m/s)	ERMS (m/s)	SI	r	Bias (m)	ERMS (m)	SI	r	Bias (s)	ERMS (s)	SI	r
42001	WNA	-0.29	2.95	0.36	0.82	0.17	0.60	0.32	0.94	-0.29	1.09	0.15	0.93
	NAH	-0.16	1.61	0.20	0.95	0.13	0.46	0.24	0.97	-0.50	1.28	0.17	0.90
42002	WNA	-0.35	1.50	0.19	0.91	-0.08	0.27	0.15	0.98	-0.83	1.22	0.12	0.94
	NAH	-0.38	1.65	0.21	0.89	-0.17	0.30	0.14	0.98	-1.01	1.25	0.10	0.96
42003	WNA	0.33	1.29	0.15	0.96	0.08	0.37	0.18	0.97	-0.76	1.34	0.15	0.86
	NAH	-0.07	1.28	0.16	0.95	-0.13	0.56	0.27	0.93	-1.05	1.69	0.18	0.80
42039	WNA	0.42	1.25	0.18	0.96	0.02	0.30	0.18	0.98	-0.14	1.67	0.24	0.72
	NAH	0.09	1.26	0.19	0.95	-0.12	0.35	0.20	0.98	-0.36	1.70	0.24	0.72
42040	WNA	0.83	1.40	0.16	0.98	0.06	0.30	0.17	0.99	-0.21	1.05	0.15	0.91
	NAH	0.40	1.21	0.17	0.97	-0.11	0.33	0.18	0.98	-0.44	1.29	0.17	0.88
42019	WNA	0.50	1.09	0.14	0.95	-0.16	0.49	0.32	0.94	-0.19	1.94	0.27	0.74
	NAH	0.49	1.15	0.15	0.94	-0.21	0.51	0.32	0.95	-0.53	2.01	0.27	0.74
42020	WNA	-0.03	0.98	0.15	0.94	-0.24	0.49	0.28	0.93	-0.29	1.99	0.27	0.73
	NAH	-0.03	1.12	0.17	0.92	-0.29	0.49	0.26	0.95	-0.53	1.83	0.24	0.79
42036	WNA	0.69	1.48	0.21	0.94	0.01	0.23	0.16	0.98	-0.06	1.44	0.22	0.74
	NAH	0.30	1.39	0.22	0.92	-0.12	0.29	0.19	0.97	-0.33	1.55	0.23	0.72

Table 2: Bulk validation statistics for the combined occurrence period of hurricanes Isidore and Lili. WNA and NAH wave modelresults are compared to observations at eight NDBC buoy locations.

buoy 42003, and appears to be related to the cumulative underestimation of Lili's NE quadrant winds by the GFDL model, which led the NAH model to generate swells that were weaker than observed at buoy 42003. This problem has been solved in a more recent version of the GFDL model (see below). At buoy 42001, which was the only buoy directly under Lili's track and, thus, exposed to extreme wind intensities, the validation statistics indicate a clear superiority of winds and waves predicted by the NAH model.

The passage of Lili over buoy 42001 occurred when the hurricane was near its maximum intensity. As shown in Figure 5(a), GFDL winds used by the NAH model reproduced more closely Lili's maximum U_{10} profile at buoy 42001 than the GFS winds in the WNA model. Still, the GFDL model underestimates the observed maximum wind speed by aproximately 20%. Such discrepancy may results from actual mesoscale variabilities in the wind field not reproduced by the GFDL model, or by innaccuracies in the location of maximum winds in a small storm such as Lili. These problems tend to be minimized in a wave model because a wave model responds more strongly to the larger time and space scales in the wind fields, and thus tends to act as a low pass filter. On the other hand, underestimated extremes model winds may also have been compensated in the wave model due to a wind stress parameterization that does not yet include the observed effects of surface drag reduction in very high speeds (Powell et al., 2003; Moon et al., 2003).

Despite these discrepancies and uncertainties, the enhanced performance of the GFDL model winds relative to the GFS model during the passage of Lili over buoy 42001 reflected positively in the validation statistics for H_s: NAH hindcast

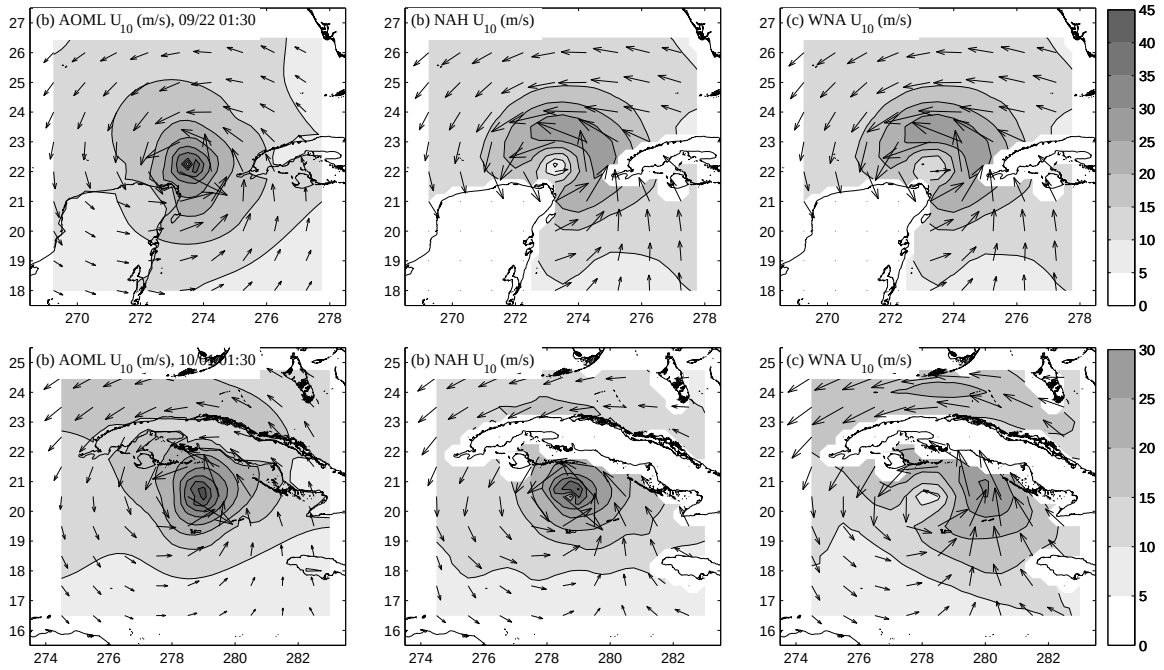

Figure 10: Comparison of AOML surface winds with NAH and WNA surface wind fields: (a) Isidore's first crossing of the Gulf of Mexico September 22nd and (b) Lili near maximum intensity on October 3rd.

of H_s were significantly better than those of the WNA model as seen in Figure 6 (a). Though not clearly reflected in statistics for T_p, this improved performance is evident in the time series for T_p near the storm peak, as seen in Figure 7. These results reveal that the NAH model provides good estimates of extreme wave conditions, which are critical in operational forecasting of hurricane waves.

A conspicuous feature in Table 2 is the comparatively poor performance of both models in terms of hindcast H_s at buoys 42019 and 42020. Through visual inspection of Figure 6, it is clear that these biases result from an under-prediction of H_s between September 24th and 27th (second stage of Isidore's passage over the Gulf of Mexico). Not by chance, the highest bias in computed T_p from both WNA and NAH models occurs for data from buoy 42002 and is closely connected with the model H_s bias in buoy 42019 and 42020 between September 26th and 27th (see Figure 7). The reason behind these more noticeable discrepancies stems largely from biases in the forcing hindcast surface wind fields used in the wave models.

Although these biases are not clearly seen in the time series of U_{10} shown in Figure 5, significant sources of biases in the spatial distribution of model wind intensities are revealed when a comparison is made against manual analyses of surface winds made at the Hurricane Research Division (AOML/HRD) of

NOAA's Atlantic Oceanographic and Meteorological Laboratory (Powell et al., 1998). An example of such bias is presented in Figure 10(a), which compares HRD-analyzed winds with surface winds used by the WNA and NAH models on September 22, 0130 UTC. Normally, the hurricane's maximum wind region is the strongest source of energy to generating swells. In this special situation, however, the presence of Cuba isolated the maximum wind region from Lili's outer flow. The HRD-analyses in Figure 10(a) indicate that model winds in Lili's outer flow were much weaker than actual winds. Consequently, simulated swell fields are significantly weaker than measurements made at buoys 42019 and 42020, as shown in Figure 6(f) and (g).

The best performance of WNA relative to NAH was recorded at buoys 42003, 42039 and 42036, all to the east of hurricane Lili's path. In these cases, the relatively poorer performance of the NAH model is associated with the generation of weaker swell systems as a consequence of weaker GFDL model winds away from the hurricane's eye (outer wind field sectors) when Lili was entering the Gulf of Mexico, north of Cuba. Figure 10(b) shows the HRD-analyzed surface winds and the wind fields used by WNA and NAH on October 1st 0130 UTC, the most likely date in which these swell systems were generated. Figure 10(b) reveals that the stronger wind sector north of Cuba observed in the HRD fields is well approximated by GFS/WNA, but significantly underestimated by the GFDL/NAH winds. This problem resulted from deficiencies in the planetary boundary layer (PBL) closure scheme used in the GFDL model until the end of the 2002 hurricane season. To eliminate this deficiency, the PBL scheme used in the GFS model was implemented onto the GFDL model (Tim Marchock, personal communication, 2004). The sensitivity of wave model predictions to these changes is discussed in Tolman et al. (2004).

6.2 Wind and Wave Forecasts

Due to the availability of hourly GFDL winds only up to the 72 h forecast horizon, our analysis of forecast performance of the NAH and WNA models will also be limited to this forecast period, even though the latter provides products up to 168h. A convenient way of summarizing the skill of wind and wave model forecasts associated with the NAH and WNA models is illustrated in Figures 11, 12, 13 and 14. These figures show the time series of envelopes bounded by maximum and minimum values of U_{10}, H_s and T_p obtained from all available forecast data ranging from 0h to 72h. Theses figures, thus, illustrate the range of variability of forecasts at selected buoy sites during the passage of Isidore and Lili through the Gulf of Mexico.

A striking feature of Figures 11 though 14 is the relatively modest envelope width, indicating a moderate range of change or variability that implies a high consistency between hindcast and forecasts up to the 72h forecast horizon. There

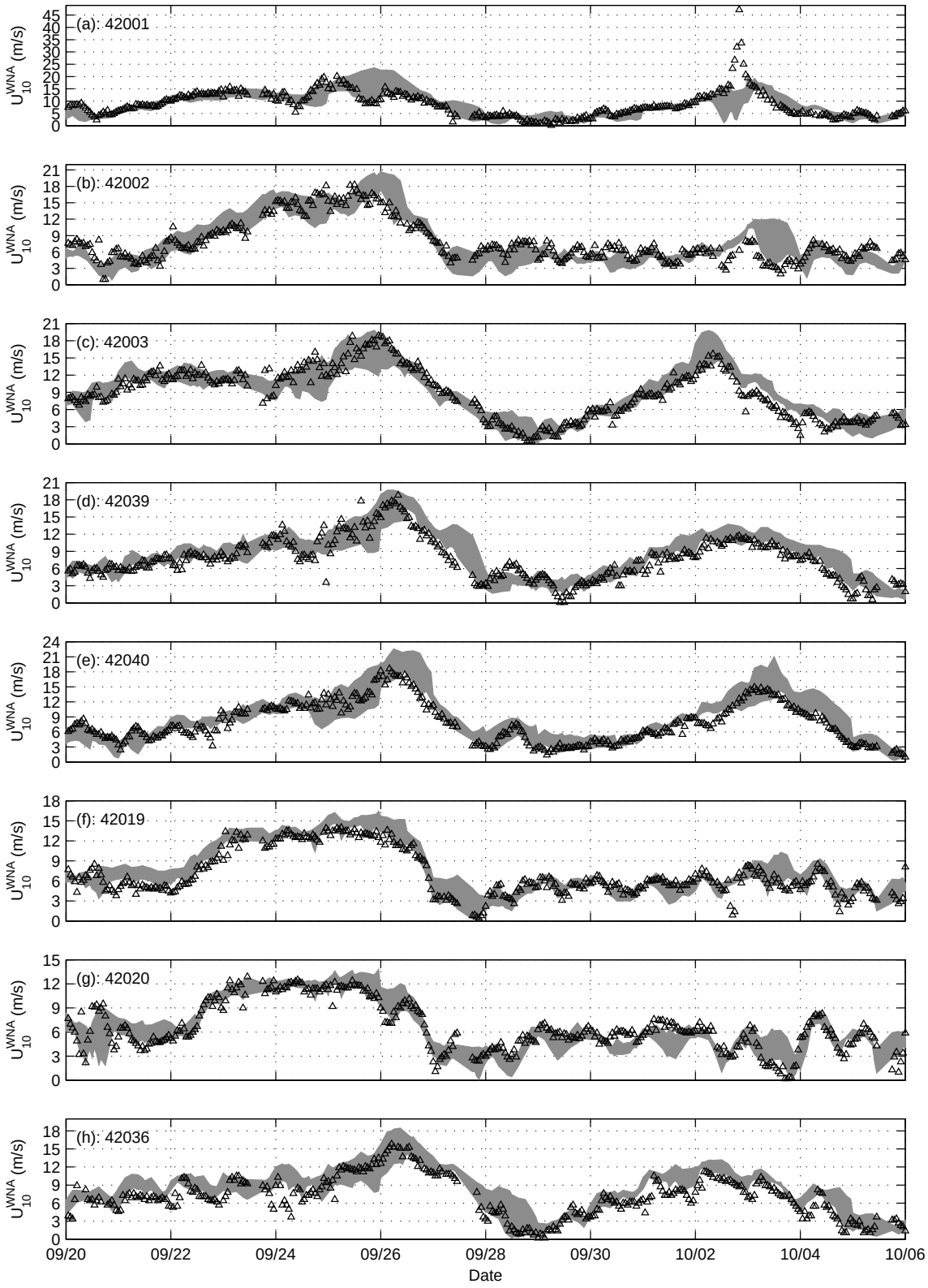

Figure 11: Time series of the forecast envelope of U_{10} from the WNA (GFS) model. The envelope is defined as the range between maxima and minima of all forecast ranges from 0h to 72h at any given time unit.

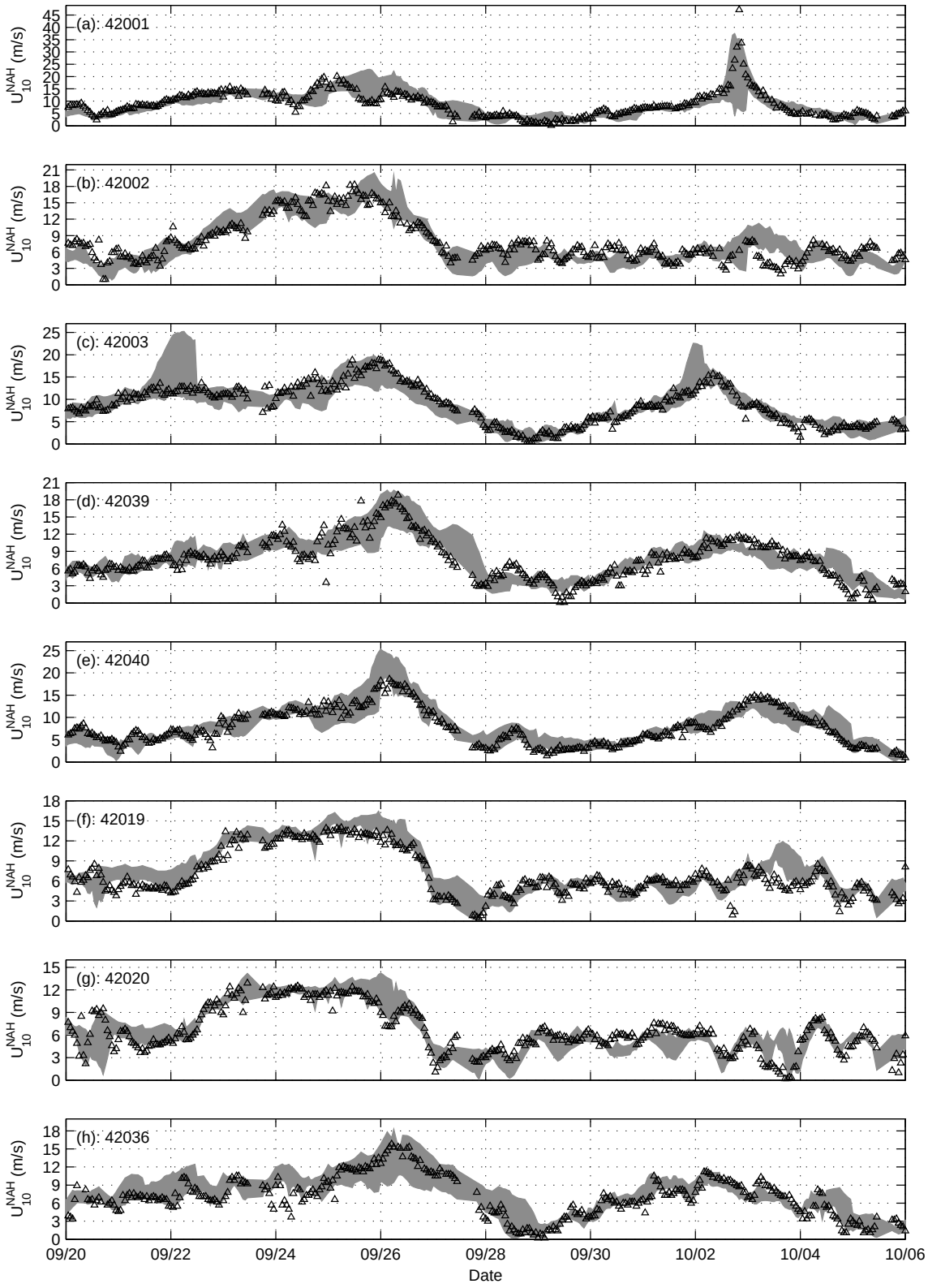

Figure 12: Forecast envelope of U_{10} from the NAH (GFDL) model.

are, however, several short sections in the diagram showing considerably large envelope widths. A careful examination indicates that these occurred near the times of arrival of windseas or swells generated by either Lili or Isidore, suggesting a large change in predicted parameters associated with these hurricanes from one forecast cycle to another. The most obvious reason for that is the expected uncertainty in atmospheric model forecasts of wind intensity within stronger storm systems, particularly in extreme and complex wind conditions associated with hurricanes.

Less obvious, but not least important, is the effect of uncertainties associated with forecasts of the path followed by the two hurricanes. An illustration of the uncertainty in model track forecasts of hurricanes Isidore and Lili relative to the best track data issued by the NCEP's National Hurricane Center (NHC) is shown in Figure 15. Envelopes of forecast tracks from the GFDL hurricane model, shown in Figure 15(a), reveals that the variability in the predicted position of both hurricanes was quite large within a forecast range of 72 h. In its widest points, the envelope indicates an uncertainty of up to 5° of latitude, which is on the order of magnitude of the size of the hurricane systems themselves. As is to be expected, uncertainties grow and the forecast track envelope widens as the forecast range grows, being relatively small and very close to the NHC best track analysis for a forecast range of 0h-24h. Forecast track envelopes from the GFS model, shown in Figure 15(b), retain most of the more relevant properties of the forecast track envelopes of the GFDL model in Figure 15(a). Again, the largest uncertainty in the location of both hurricanes is on the order of 5° of latitude.

Despite the general similarity, Figure 15 reveals track differences that could potentially affect the wave model forecasts of the WNA and NAH models and explain some of their differences. A comparison between panels (a) and (b) indicates that the uncertainty in GFS forecast tracks for hurricane Isidore was slightly smaller than that of GFDL forecasts in both the 24h-48h and 48h-72h ranges. The difference was particularly large near buoy 42003, mostly in the 48h-72h ranges, and in the approach to Isidore's final landfall in the Louisiana coast. The higher inaccuracy of GFDL's 48h-72h range forecast in predicting Isidore's approach to buoy 42003 explains the very wide forecast envelope of H_s near September 22nd, in the time series for the NAH model, as shown in Figures 11(c) and 12(c). It may also be related to the wider envelopes in NAH forecast envelopes at buoys 42036 and 42039 on September 22nd.

Most differences observed in forecast track envelopes during hurricane Lili for the GFS and GFDL model occurred before the storm entered the Gulf of Mexico, as suggested by Figure 15. Consequently, the differential effects of track position uncertainties in this case seem to have been overpowered by the more significant differences in the intensity of surface wind fields in the Gulf, as described in previous sections.

Figures 16 and 17 show the validation statistics of U_{10}, H_s and T_p associated

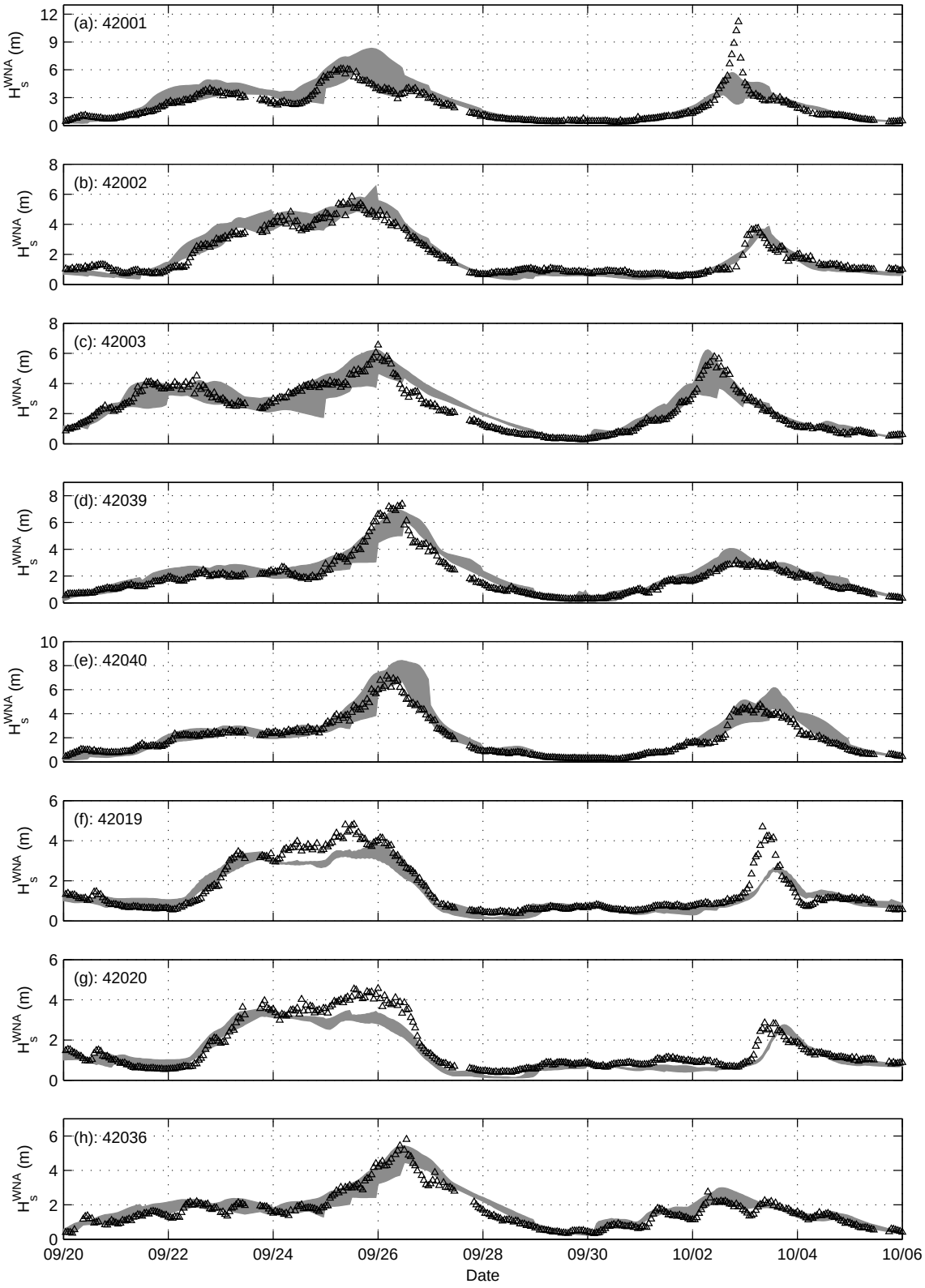

Figure 13: Forecast envelope of H_s from the WNA model.

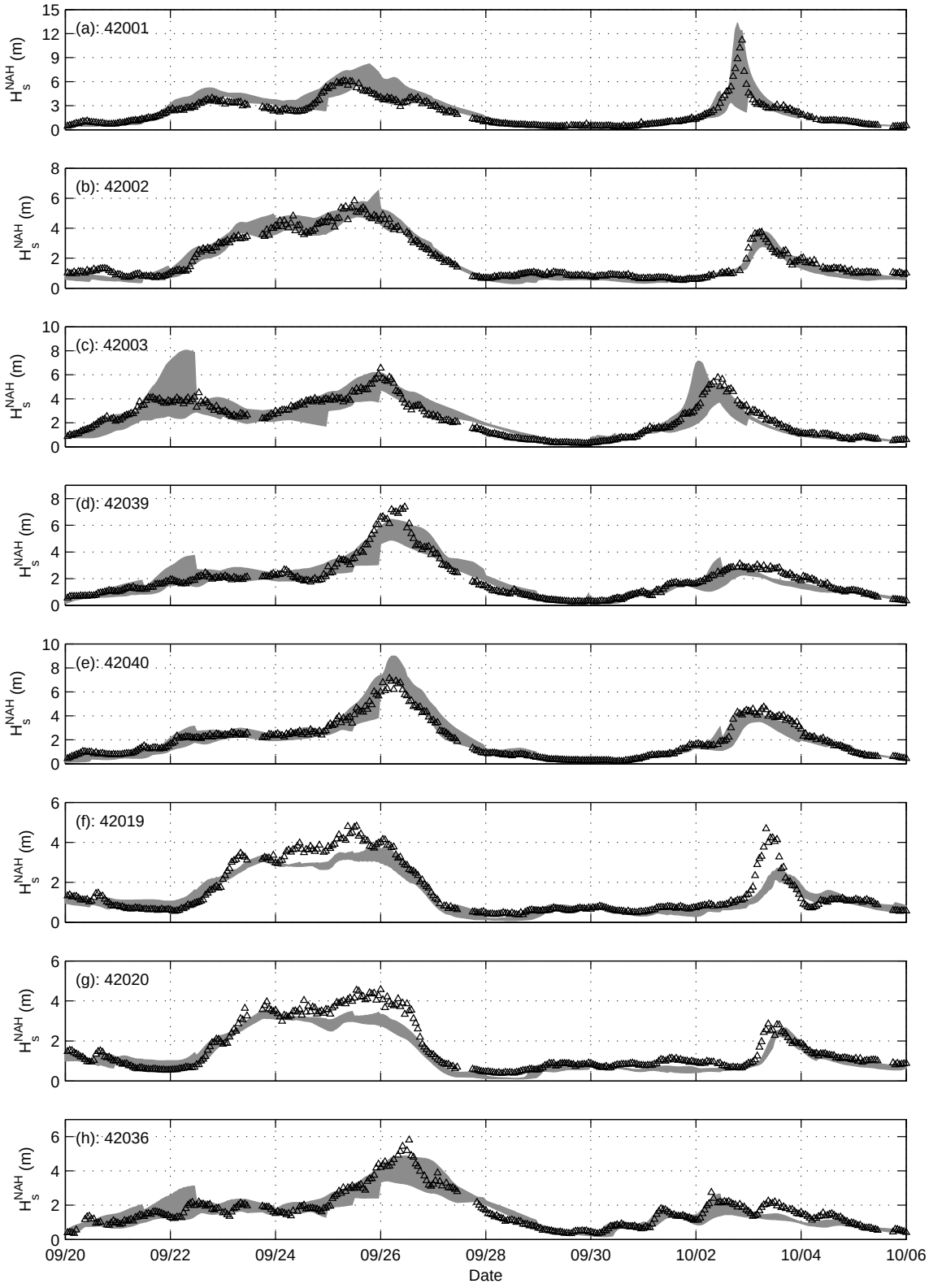

Figure 14: Forecast envelope of H_s from the NAH model.

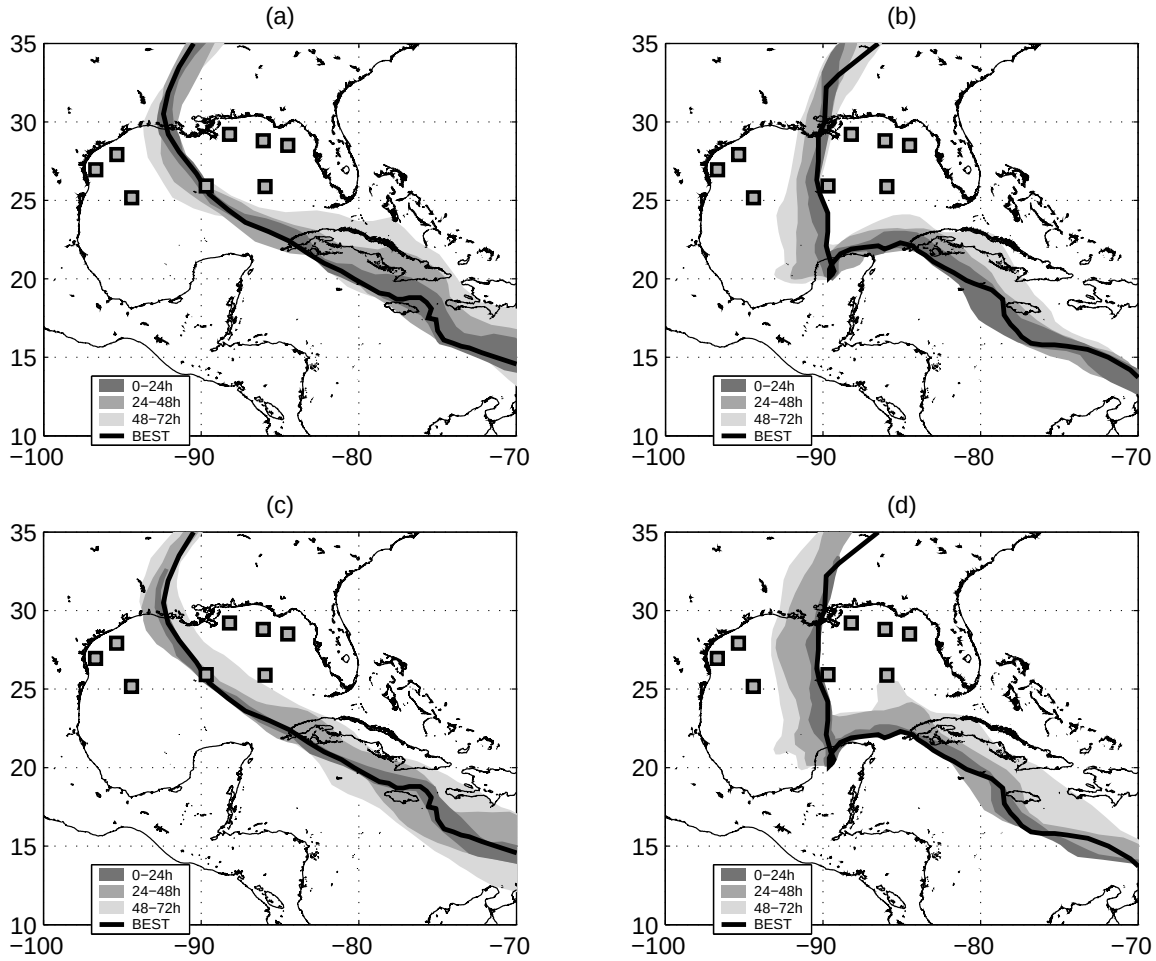

Figure 15: Track envelopes for hurricanes Lili and Isidore from the WNA and NAH models at several forecast ranges from 0h to 72h, shown with the best track data from NOAA's National Hurricane Center. Tracks from the WNA (GFS) model are shown in panels (a) and (b), while NAH (GFDL) model tracks are shown in panels (c) and (d) for hurricanes Lili and Isidore, respectively.

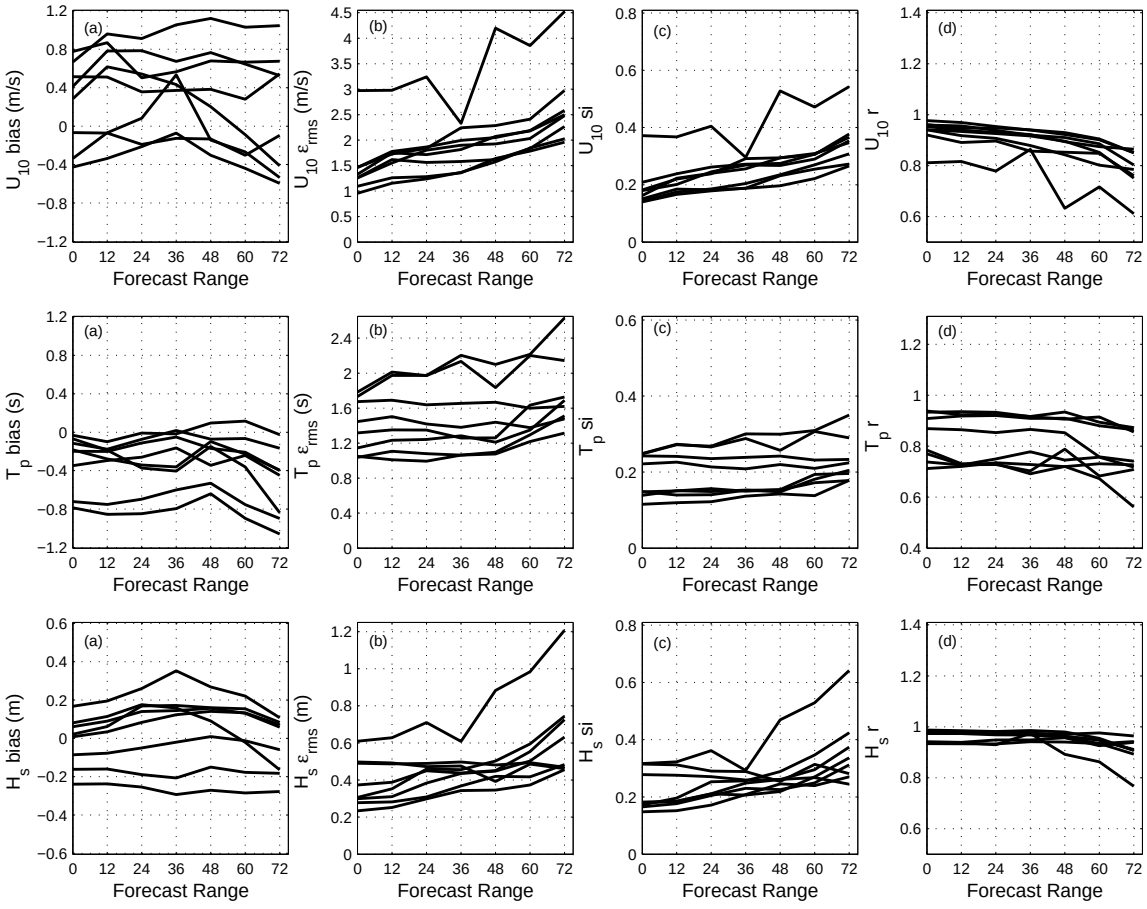

Figure 16: Diagram showing evolution of validations statistics for the WNA model at all buoy locations over a forecast horizon of 72h: (a) bias, (b) RMS error, (c) scatter index and (d) correlation coefficient.

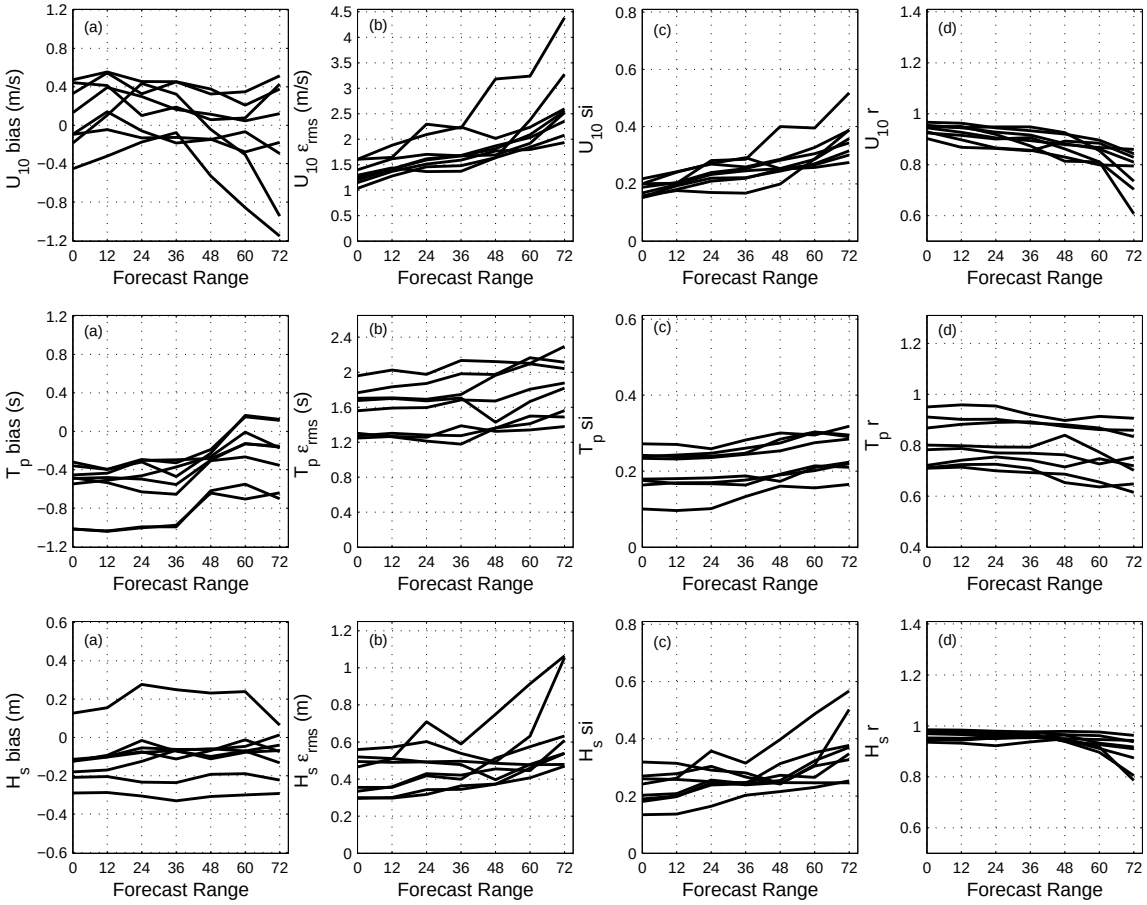

Figure 17: Diagram showing evolution of validations statistics for the NAH model at all buoy locations over a forecast horizon of 72h: (a) bias, (b) RMS error, (c) scatter index and (d) correlation coefficient.

with the WNA and NAH models, respectively, as a function of projected forecast hours: 0h, 12h, 24h, 36h, 48h, 60h and 72h. These figures provide a detailed view of the 'drift ' in model skill as the forecast range increases from 0h to 72h. The deterioration of forecasts skill for U_{10}, H_s and T_p for longer forecast projection hours is clearly indicated by gradually increasing values of Erms and SI and decreasing correlation coefficients (r) as shown in these figures. It also can be seen from these figures, particularly from the values of model bias, that both models present comparable statistical scores with the NAH model slightly outperforming WNA in this forecast range.

6.3 Forecasts of Extreme Storm Conditions

A major concern in an operational wave forecasting system is the ability to forecast extreme sea state conditions during hurricanes. For this reason, in this section we dedicate special attention to investigating the performance of wave forecasts relative to buoy measurements of storm maxima. A visual inspection of Figure 6 suggests that during hurricane Isidore both NAH and WNA models had only small differences in forecasts of storm peaks. On the other hand, the differences were significant during hurricane Lili. Therefore, our analysis of model performance in terms of predicting extreme sea states will focus on wave fields associated with Lili.

To assist in our evaluation of wave model forecasts, we introduce a convenient way of summarizing their ability to predict storm maxima using a "target" diagram, as shown in Figure 18. The interpretation of this diagram is as follows. We first define acceptable ranges of bias and time lags of model predictions of maximum H_s relative to buoy data, which were chosen presently to be $\pm$ 20 % and $\pm$ 3 h. We then define the "target" as a box indicating a region of values satisfying these criteria.

Target plots for the following forecast ranges of maximum waves during hurricane Lili are shown in Figure 18: -6h-0h, 0h-12h, 12h-24h and 36h-48h. Target diagrams for the WNA and NAH models are shown in the left- and right-hand side panels, respectively. The list of symbols used to represent biases and time lags at each buoy location is provided in the figure caption. Biases are defined as the relative difference between the highest modeled and measured H_s within the envelope of wave heights associated with Lili. Time lags are the time displacements between modeled and observed storm envelopes with higher correlation coefficient.

Figure 18 indicates that forecasts of storm maxima provided by the NAH model were generally within or very near the acceptable $\pm$ 3 h range up to the 48h forecast horizon. WNA model predictions were also on target in terms of time lags, but had a somewhat larger scatter, particularly at larger forecast horizons. WNA data at two buoy locations fell clearly outisde the tolerance bounds, whereas all NAH data were within or very near the acceptable bounds. In terms of biases, the cloud of data points from both models seem to indicate that they had similar overall performance. However, a closer look at the data reveals important differences.

Buoy 42001 was the only location directly under Lili's track to provide data representing extreme wave heights generated by Lili. Figure 18 shows that the NAH hindcast of maximum wave height at this location (H_s=11.6 m) predicted the measured storm maximum wave height (H_s=11.2 m) with excellent accuracy in both time of occurrence and intensity. Conversely, the WNA model hindcast (H_s=5.7 m) under-predicted significantly the observed wave height at this buoy location.

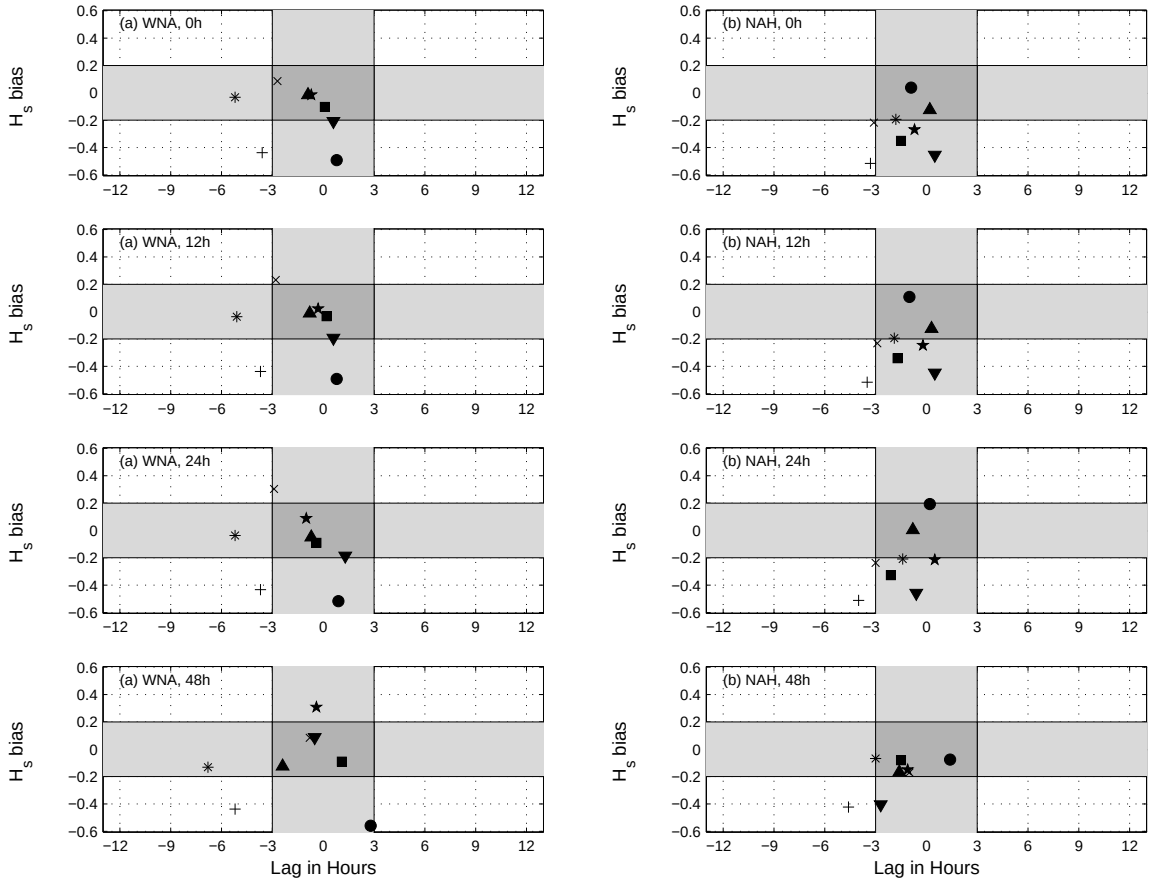

Figure 18: Diagram indicating the accuracy of the NAH model in predicting the maximum waves generated by hurricane Lili at and relative to selected NDBC buoy locations. Buoy patterns: 42001 (•), 42001 (▲), 42003 (■), 42039 (★), 42040 (×), 42019 (+), 42020 (∗) and 42036(▼).

The excellent performance of the NAH in predicting these highest measured waves generated during both Isidore and Lili resulted from the very good description by the GFDL model of the hurricane's wind field near its region of maximum winds. Conversely, the poorer performance of the WNA model resulted from the intrinsic inability of the GFS model in predicting winds near the core of a hurricane system.

Although NAH hindcasts of H_s slightly under-predicted the measured storm maxima at most other buoy locations, the differences between the NAH and WNA models were less evident than at buoy 42001. These other buoy locations were mostly exposed to swell systems rather than local windseas coupled to Lili's maximum wind region. The better performance of the WNA model in these cases is related to the fact that the GFS model provided a better description of winds in Lili's far-field regions, i.e. regions around the hurricane but far away from the maximum wind core. This is particularly evident in Figure 18 for buoy 42003, where the WNA model clearly outperforms the NAH model at all forecast times.

Our comparisons of surface winds against analyzed data indicated that the GFDL model generally produced weaker far-field winds than the GFS model, which led to the generation of weaker swell. This misrepresentation of far-field hurricane winds, found in the 2002 hurricane season data, seems to have been reduced by changes in the GFDL physics package, with positive impacts to hurricane predictions, as shown in Tolman et al. (2004).

This page is intentionally left blank.

7 Discussion

The main reason for running specialized hurricane wave models is the possibility to use driving winds with higher resolution in space and time, generated by an atmospheric model developed specifically for hurricane prediction (e.g., the GFDL model). This is particularly important because the GFS model used to drive most wave models at NCEP does not have sufficient resolution to realistically represent the circulation of small tropical systems.

The basic concept of NCEP's operational hurricane wave models is to use a blended wind field. This consists of a combination of higher resolution GFDL wind fields around hurricanes with GFS winds in the outer region not directly under a hurricane's influence. NCEP has pioneered specialized hurricane wave modeling, and to our knowledge, still is the only operational weather center providing forecast data generated by specialized hurricane wave models.

NCEP's hurricane wave models require availability of the wind fields from one or more runs of the GFDL model. Because the GFDL model uses boundary conditions generated by the GFS model, it is scheduled to run only after the conclusion of a complete GFS run cycle. The NAH wave model in turn needs to wait for the conclusion of all GFDL model runs before it can be started. The operational products from the NAH model, therefore, are always available much later that the output of the WNA model. Because operational wave forecasters require these 'early' results generated by the WNA model for many products, the NAH model is run next to the WNA model, instead of replacing it.

In the present manuscript, we illustrate the performance of the NAH model for the 2002 Atlantic hurricane season, using results for hurricanes Isidore and Lili in the Gulf of Mexico. Conventionally, wave model validation is performed for long periods and many observation platforms. Such a comparison between the WNA and NAH models is not relevant, because significant differences occur only for a small number of hurricanes, and mostly for observations relatively close to the track of the hurricanes. Such differences are generally lost in bulk statistics for longer periods. Hence, case studies are more relevant for model comparison and validation. Case studies, such as the ones presented here, also identify the complexity of wave conditions generated by an intense hurricane.

It is expected that differences between conventional and hurricane wave models will vary significantly from hurricane to hurricane. Isidore was a very large hurricane, which was well resolved by the GFS. Therefore, GFS and GFDL wind fields were very similar and, consequently, the WNA and NAH models showed virtually identical wave fields. Lili, on the other hand, was small and intense. The GFS model did not resolve and represent Lili's wind fields well, whereas the GFDL model resulted in much more realistic wind conditions. Consequently, extreme waves were much better represented in the NAH model than in the WNA model. It is also clear that the most conspicuous wave model deficiencies, partic-

ularly the underestimation of the swell heights from Isidore in the western Gulf in both the WNA and NAH models (Fig. 6, between the 24th and 26th of September) and during Lili for the NAH model at buoy 42003, appears to be associated with deficiencies in the wind forcing provided by the atmospheric models.

The WNA and NAH models showed nearly identical results for hurricane Isidore, when both models equally suffered from using forecast wind fields that did not agree well with analyzed data. Therefore, the remainder of this discussion will focus on hurricane Lili, when the different properties of both models seemed more enhanced. Buoy data measured during Lili also provided a wider range of wave evolution scenarios, including extreme waves recorded when the hurricane's maximum wind region moved directly over buoy 42001, in the center of the Gulf of Mexico.

Maximum wave heights observed at buoy 42001 (11.2 m), were very well represented by the hindcast of the NAH model (11.6 m), but severely underestimated by the WNA model (5.7 m). The reason for this was the much more realistic description of the core and high wind speed area of Lili by the NAH (GFDL) model, as previously discussed. The top panel in Figure 14, indicates that the wave forecasts close to the 72 hour range were not capturing Lili well. However, this was mostly due to deficiencies in the later forecast ranges. On the other hand, the maximum wave heights at buoy 42001 in the 24 and 48 h forecasts were 12.4 m and 12.5 m, respectively. In both cases the occurence time of storm maxima were predicted within 3 hours of the observed maximum wave height time of occurence. Hence, the NAH model provided accurate guidance for Lili out to the 48-hour forecast.

Despite the clear superiority of the NAH model in predicting extreme wave heights at buoy 42001 during Lili, statistics shown in Table 2 indicate that both WNA and NAH models performed rather poorly at most other buoy locations. The low resolution GFS winds may explain the poor performance of the WNA model in most situations. One possible explanation for the poor performance of the NAH model, particularly in predicting swell recorded at buoys located away from Lili's path, is the fact that the NAH model hindcast uses GFS analyses blended with short term *forecasts* from the GFDL model, which does not generate analyzed fields.

Another issue that may be a limiting factor for the accuracy of NAH model forecasts is the wave model itself. It is well known that the existing parameterizations of many wave growth physical processes rely on empirical tuning to be accurate, even in the most advanced numerical wave models. The tuning of the WAVEWATCH III model has been performed using wind forcing provided by the GFS model and its predecessors. Therefore, it may well be that this tuning is not optimal for more accurate hurricane winds.

It is also well known that present parameterizations of wave physics tend to over estimate the directional width of spectra. This is expected to have the biggest

impact on model results in wind conditions with rapidly changing wind directions, as observed near the core of a hurricane. Furthermore, the parameterizations of wave-growth physics used in wave models are based on relatively moderate wind conditions. Recent research (e.g., Powell et al., 2003; Moon et al. 2004) indicates that the extrapolation of these parameterizations to hurricane conditions will lead to an overestimation of surface stresses. This will, therefore, have an impact on wave growth rates, model behavior and potentially model tuning.

The limitations identified above have been the subject of ongoing wind-wave research activities at NCEP. Also, our results indicate that wave model research may provide a framework for further improvements, particularly from the perceived need for coupling ocean, wave and wind models for accurate hurricane forecasting in general (e.g., Bender and Ginnis, 2000; Bao et al, 2000, Moon et al, 2004).

Research at NCEP has also focused on the improvement of parameterizations used in wave models to represent the physics of wave evolution. Some of this research has been explicitly geared to physical processes in hurricane conditions. We believe this framework should provide the means of overcoming some limitations highlighted in the present study.

This page is intentionally left blank.

8 Summary and concluding remarks

This paper describes NCEP's North Atlantic Hurricane (NAH) wave model. This model is compared to the conventional Western North Atlantic (WNA) model for two severe Atlantic hurricanes in 2002, Isidore and Lili. Both models are validated using buoy data provided by NOAA's National Data Buoy Center (NDBC).

Our main conclusions are:

- Blending high-resolution, regional GFDL wind and low-resolution, global GFS surface winds provides a proper framework for predicting hurricane waves.

- The use of case studies provides an effective framework for assessing model performance and incorporate important improvements to hurricane wave forecasting systems.

- Specific properties of hurricane systems, particularly their size, have a strong impact on the quality of surface wind fields generated by the GFS and GFDL models.

- Maximum winds are generally well captured by the GFDL model. However, in large systems such as Isidore the GFS model appeared to provide better winds in the outer sector of the hurricane, with a positive impact on generating swell systems. The poorer outer wind-field from GFDL model was somewhat anomalous for Lili. A recent GFDL model release which has minimized this problem is now presently used to force NCEP's hurricane generated wind-wave models.

- The use of blended GFS/GFDL winds can produce accurate forecasts of extreme wave heights associated with intense hurricane out to the 48-hour forecast range, despite innaccuracies in maximum surface wind intensity and location. This may reflect wave growth mechanisms which tend to attenuate small-scale variability in the wind field, but may also result from underestimated maximum GFDL winds being compensated by overestimated surface drag for high winds in the wave model. This important issue is being investigated further as improvements are made to NCEP's wind and wave models.

The performance analysis presented in this study sets the framework for improvements to be incorporated in future implementations of hurricane wave forecasting models at NCEP. These include, potentially, increasing the spatial resolution of wave models in areas under hurricane force winds poissibly using multiscale grid systems, coupling waves and wind fields, and incorporating data assimilation for generating surface wind analyzes in operational GFDL model

cycles. These issues are currently the object of ongoing research acitivities at NCEP.

This page is intentionally left blank.

References

Avila, L.A., 2002: *Tropical Cyclone Report: Hurricane Isidore, 14 - 27 September 2002*, National Hurricane Center, NOAA, USA, http://www.nhc.noaa.gov/2002isidore.shtml (20 Dec. 2002).

Bao, J.-W., J.M. Wilczak, J.-K. Choi and L. H. Kantha, 2000: Numerical simulations of air-sea interaction under hight wind conditions using a coupled model: A study of hurricane development, *Monthly Weather Review*, **128**, 2190-2210.

Barber, N.F. and F. Ursell, 1948: The generation and propagation of ocean waves and swell. I. Wave periods and velocities, *Trans. R. Soc. London*, **240(A)**, 527-560.

Bender, M.A. and I. Ginis, 2000: Real-case simulations of hurricane-ocean interaction using a high-resolution coupled model: effects on hurricane intensity, *Monthly Weather Review*, **128**, 917-946.

Bender, M.A., I. Ginis, T.P. Marchok and R.E. Tuleya, 2001. Changes to the GFDL hurricane forecast system for 2001 including implementation of the GFDL/URI hurricane-ocean coupled model. Technical Procedures Bulletin No. 472B, National weather Service, NOAA, U.S. Department of Commerce.[3].

Bender, M.A., T.P. Marchok and R.E. Tuleya , 2002. Changes to the GFDL hurricane forecast system for 2002 including implementation of the 2-nested grid configuration. Technical Procedures Bulletin No. 492, National weather Service, NOAA, U.S. Department of Commerce. [4]

Caplan, P., J. Derber, W. Gemmill, S., -Y. Hong, H.,-L. Pan and D. Parish, 1997: Changes to the NCEP operational medium-range forecast model analysis/forecast system. Wea. Forecasting, **12**, 581-594.

Cardone, V.J., R.E. Jensen, D.T. Resion, V.R. Swail and A.T. Cox, 1996: Evaluation of contemporary ocean wave models in rare extreme events: the Halloween storm of October 1991 and the storm of the century of March 1993. *J. Atm. Ocean. Tech.*, **13**, 198-230.

Chao, Y. and H. Tolman, H. 2000: Numerical experiments on predicting hurricane generated wind waves. Preprints of the 6th International Workshop on Wave Hindcasting and Forecasting, Monterey, California, November 6-10, 2000, 167-179.

[3]http://www.nws.noaa.gov/om/tpb/

[4]http://www.nws.noaa.gov/om/tpb/

Chao, Y.Y. and Tolman, H.L. 2001a: Implementation of the North Atlantic Hurricane wind wave forecasting system. Presented at a NWS CAFTI Meeting, May 24, 2001 unpublished.

Chao, Y. and H. Tolman, H. 2001b: Specification of hurricane wind fields for ocean wave prediction. Ocean Wave Measurement and Analysis, Proc. 4th International Symposium Waves 2001, Vol. 1, 671-679.

Chao, Y., L. Burroughs L., and Tolman, H. 1999a: Wave Forecasting for Alaskan waters. Technical Procedures Bulletin No. 496, National weather Service, NOAA, U.S. Department of Commerce.[5].

Chao, Y., L. Burroughs L., and Tolman, H. 1999b: Wave Forecasting for the western North Atlantic and Adjacent Waters. Technical Procedures Bulletin No. 495, National weather Service, NOAA, U.S. Department of Commerce.[6]

Chao, Y., L. Burroughs L., and Tolman, H. 2001: The North Atlantic hurricane wind wave forecasting system. Technical Procedures Bulletin No. 478, National Weather Service, NOAA, U.S. Department of Commerce. [7]

Chao, Y., L. Burroughs L., and Tolman, H. 2002: Wave Forecasting for the eastern North Pacific and Adjacent Waters. Technical Procedures Bulletin No. 491, National Weather Service, NOAA, U.S. Department of Commerce. [8]

Kanamitsu, M., J. C. Alpert, K. A. Campana, P. M. Caplan, D. G. Deaven, M. Iredell, B. Katz, H. -L. Pan, J. E. Sela, and G. H. White, 1991: Recent Changes implemented into the global forecast system at NMC. Wea. Forecasting, 6, 425-435.

Kurihara, Y., and M. A. Bender, 1980: Use of a movable nested mesh model for tracking a small vortex. Mon. Wea. Rev.108, 1792-1809.

Kurihara, Y., M.A. Bender, R.E. Tuleya and R.J. Ross, 1990: Prediction experiments of Hurricane Gloria (1985) using a multiply nested movable mesh model. Mon. Wea. Rev., 118, 2185-2198.

Kurihara, Y., M.A. Bender, R.E. Tuleya and R. J. Ross, 1995: Improvements in the GFDL hurricane prediction system. Mon. Wea. Rev., 123, 2791-2801.

[5]http://polar.wwb.noaa.gov/omb/tpbs/tpb496
[6]http://polar.wwb.noaa.gov/omb/tpbs/tpb495
[7]http://polar.wwb.noaa.gov/omb/tpbs
[8]http://polar.wwb.noaa.gov/omb/tpbs/tpb491

Kurihara, Y., R.E. Tuleya and M. A. Bender, 1998: The GFDL hurricane prediction system and its performance in the 1995 hurricane season. Mon. Wea. Rev., 126, 1306- 1322.

Lawrence, M.B., 2002: *Tropical Cyclone Report: Hurricane Lili, 21 September - 04 October 2002*, National Hurricane Center, NOAA, USA, http://www.nhc.noaa.gov/2002lili.shtml (3 April 2003).

Leonard, B.P., 1979: A stable and accurate convective modeling procedure based on quadratic upstream interpolation. Comput. Methods Appl. Mech. Engng. 19, 59-98.

Leonard, B.P., 1991: The ULTIMATE conservative difference scheme applied to unsteady one-dimensional advection. Comput. Methods Appl. Mech. Engng.,88, 17-74.

Liu, Q., T. Marchok, Pan H-L, B. Morris and S. Lord, 2000: Improvements in hurricane initialization and forecasting at NCEP with global and regional GFDL models. Technical Procedures Bulletin No. 472, National weather Service, NOAA, U.S. Department of Commerce. [9]

Moorthi, S., H.-L. Pan and P. Caplan, 2001: Changes to the 2001 NCEP operational MRF/AVN global analysis/forecast system. Technical Procedures Bulletin No. 484, National weather Service, NOAA, U.S. Department of Commerce. [10]

Moon, I.J., T. Hara, I. Ginnis, S.E. Belcher and H. L. Tolman,: 2004: Effect of surface waves or air-sea momentum exchange: I. Effect of mature and growing seas, Submitted.

Munk, W.H., 1947: Tracking storms by forerunners of swell. J. Meteorol. 4(2): 45-57.

Snodgrass, F.E., G.W. Groves, K.F.Hasselmann, G.R. Miller, W.H.Munk and W.H. Powers, 1966: Propagation of swell across the Pacific. *Trans. R. Soc. London*, **259(A)**, 431-497.

Surgi, N., H.-L. Pan and S.J. Lord, 1998: Improvement of the NCEP global model over the tropics: an evaluation of model performance during the 1995 hurricane season. Mon. Wea. Rev. 126, 1287-1305.

Tolman, H.L., 1998: Validation of NCEP's ocean winds for the use in wind wave models, *Global Oc. Atmos. Syst.*, **6**, 243-268.

[9] http://www.nws.noaa.gov/om/tpb/
[10] http://www.nws.noaa.gov/om/tpb/

Tolman, H.L., 1999: User manual and system documentation of WAVEWATCH-III version 1.18. Tech. Note. No.166, Ocean Modeling Branch, NCEP/NWS/NOAA, U.S. Department of Commerce, 110 pp. [11]

Tolman, H.L., 2002: Testing of WAVEWATCH III version in NCEP?s NWW3 ocean wave model suite. Tech. Note. No. 214, Ocean Modeling Branch, NCEP/NWS/NOAA, U.S. Department of Commerce, 99 pp. [12]

Tolman, H. L. and D.V. Chalikov, 1996: source terms in a third-generation wind wave model. J. Phys, Oceanogr. 18,1775-1810.

Tolman, H.L., B Balasubramaniyan, L.D. Burroughs, D.V. Chalikov, Y.Y. Chao, H.S. Chen, and V.V Gerald, 2002: Development and Implementation of wind-generated ocean surface wave models. Wea. Forecasting, 17, 311-333.

[11] http://polar.wwb.noaa.gov/waves/wavewatch/
[12] http://polar.wwb.noaa.gov/waves/wavewatch/